THE UNIVERSITY OF QUEENSLAND

Bismuth Telluride Based Thermoelectric Materials:

Structural Characteristics, Synthesis Processes and

Thermoelectric Properties

Student Name: Xiaofang ZENG (44048798)

Course Code: ENGG7281

Supervisor: Associate Professor Zhi-Gang CHEN and Professor Jin ZOU

Submission Date: 27 October 2017

Faculty of Engineering, Architecture and Information Technology

Abstract

Rapid population growth has led to increasing energy shortages, and these shortages will continue to rise in the future. Thus, it is urgent to figure out practical solutions to this issue. Indeed, thermoelectric power generation can be a potential candidate to this problem, but the efficiency of thermoelectric devices remains very low, which limits their applications in electricity generation. Therefore, it is necessary and important to gain deep understanding on thermoelectric materials before they can find large-scale applications. The objective of this thesis is to review Bi_2Te_3-based thermoelectric materials that exhibit good thermoelectric performance near room temperature since power generation is operated near room temperature. It is found that Bi_2Te_3 and its alloys exhibit layered structure and narrow band gap, which are favourable for high thermoelectric performance, and point defects as well as anisotropy in Bi_2Te_3-based thermoelectric materials can be used to optimize their thermoelectric performance. In addition, various simple and cost-efficiency synthesis processes can be employed to prepare Bi_2Te_3-based thermoelectric materials, including solvothermal/hydrothermal method, physical and chemical deposition (magnetron sputtering, thermal evaporation, flash evaporation and electrochemical deposition), and high-energy ball milling. Furthermore, maximizing carrier concentration (doping and point defects), optimizing carrier mobility (reconstructing random crystal lattice), Seebeck coefficient improvement (energy filtering effect) and thermal conductivity reduction (nanostructuring engineering and nanoporous structures) can contribute to enhancing thermoelectric performance of Bi_2Te_3-based materials. Finally, current challenges, possible research opportunities and recommendations will be presented in the conclusion.

Acknowledgements

Firstly, I want to express my appreciation to my project supervisors, Dr Zhi-Gang Chen and Professor Jin Zou due to their helpful advice and supportive attitude. They were very patient to guide me how to write a scientific essay and encouraged me to challenge myself when I faced problems. In addition, my supervisors gave me various access to resources related to my thesis, which helped me to successfully complete my thesis.

Secondly, I want to appreciate my thesis project PhD colleagues for their assistance and expertise.

Thirdly, I am deeply grateful for support from my family and friends because they often encouraged me to face challenges and supervised me to catch my deadline.

Finally, I want to appreciate all people who have provided me with direct or indirect assistance over the whole period of my thesis project.

Table of Contents

List of Figures

List of Tables

List of Appendices

1.   Introduction

Extensive research work has been conducted on Bi_2Te_3-based thermoelectric materials because they can exhibit high performance in conversion between waste heat and electricity energy. This review intends to present a comprehensive and critical summary of structural characteristics and synthetic methods of different Bi_2Te_3-based thermoelectric materials. In addition, this review will summarize and evaluate current practical strategies to enhance the thermoelectric performance of Bi_2Te_3-based materials. Finally, by presenting challenges and opportunities, this review will provide some possible suggestions on thermoelectric property improvement of Bi_2Te_3-based materials and offer some recommendations on the future research work, which would accelerate the extensive applications of Bi_2Te_3-based thermoelectric materials.

1.1.   Background

There has been an important growth in the global population over the last century, and this rapid population growth results in various challenging problems, including the energy crisis.[1] The energy demand will continue to considerably increase during the following decade,[2] but the use of nonrenewable fossil resources is the most common method to meet the ever-increasing energy claim, which contributes to many environmental issues such as global warming and air pollution. Therefore, research and study on reliable solutions to these challenges are very important and urgent. In fact, thermoelectric devices can be a promising approach because thermoelectric systems can directly convert waste heat, such as heat from vehicles and plants, into electricity energy.[3] Figure 1(a) is a conceptual model of thermoelectric devices, which can convert temperature differences into voltage. Thermoelectric devices consist of an array of thermoelectric modules (shown in Fig. 1(b)) in series to achieve large voltage and in parallel to achieve large current. Thermoelectric couple, also known as thermoelectric module, is made up of n-type and p-type thermoelectric materials. Electrons serve as the main charge carriers in n-type thermoelectric materials, meanwhile holes serve as the main charge carriers in p-type thermoelectric materials. As shown in Fig. 1(b), if there is a temperature difference on the

thermoelectric module, the charge carriers (electrons and holes) will move from hot to cold ends, which results in voltage produced, which is referred as Seebeck effect.
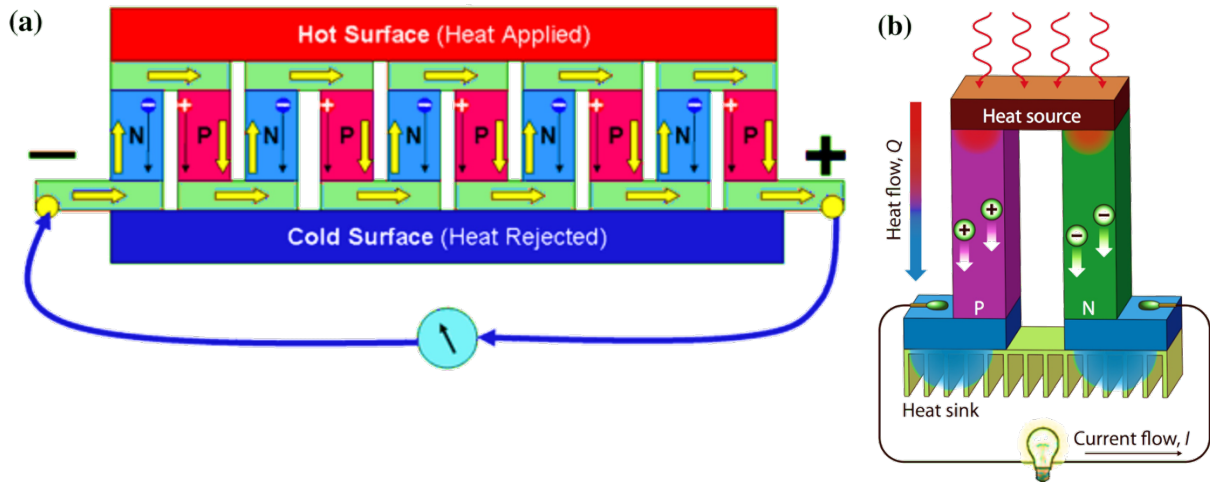
Figure 1. Conceptual illustrations of (a) thermoelectric generator and (b) thermoelectric generation module.[4,5]

In theory, thermoelectric systems can realize the conversion between waste heat and electricity energy, and Seebeck effect serves as the foundation of this type of energy conversion. Compared with tradition electricity generation, thermoelectric devices exhibit many competitive virtues, such as no moving parts, long life, fewer maintenance requirements, high reliability and no toxic gas emissions.[6] In addition, the extensive investigation on thermoelectric materials has lasted for almost one century and thus, thermoelectric generators can be a reliable method to produce electricity power. However, in practice, their unsatisfying energy conversion efficiency restricts their extensive thermoelectric power generation applications.

Low efficiency in thermoelectric power generators originates from their low dimensionless thermoelectric figure of merit, ZT, which is calculated by

$$ZT = \frac{S^2 \, \sigma \, T}{\kappa}, \tag{1}$$

where S, σ, T, and κ are Seebeck coefficient, electrical conductivity, absolute temperature and thermal conductivity respectively. Thermal conductivity, κ, in Eq.(1), results from three types of thermal conductivity: electronic, lattice and bipolar thermal conductivity. Thus, total thermal conductivity, κ, is calculated by

$$\kappa = \kappa_e + \kappa_L + \kappa_b, \tag{2}$$

where κ_e, κ_L and κ_b are electronic, lattice and bipolar thermal conductivity respectively.[7,8] Previous studies indicate that the value of ZT is limited to approximately 1 due to the interdependent relationships between transport properties and thermopower, although most thermoelectric materials can theoretically achieve a ZT as high as like. For example, CuInTe$_2$ shows a ZT of only 0.58 at 600 K.[8] Search on new thermoelectric materials with large ZT is needed to spread the use of thermoelectric power generators. Alternatively, efforts to enhance ZT of existing materials are also needed. Doping and nanostructuring are often employed to enhance thermoelectric performance of various materials.[3] For instance, doped Tl$_{0.02}$Pb$_{0.98}$Te has obtained a ZT of 1.5 at 800 K,[9] and nanostructured Si$_{0.95}$Ge$_{0.5}$ has achieved a ZT of 0.95 at 900 K.[10] p-type Bi$_x$Sb$_{2-x}$Te$_3$ and n-type Bi$_2$Te$_{3-y}$Se$_y$ have attracted the most attention because they exhibit the highest thermoelectric performance at temperatures ranging from 200 to 400 K.[11,12] Intensive study on enhancing the electron and phonon transport properties of Bi$_2$Te$_3$-based thermoelectric materials has led to considerable improvement in their ZT values,[13] which enables these thermoelectric materials to find practical applications in thermoelectric power generation. For instance, p-type Bi$_2$Te$_3$/Sb$_2$Te$_3$ superlattice devices can achieve a maximum ZT as high as 2.4 which originates from the balance between transports of phonons and electrons in the superlattice.[14] However, it remains necessary to further investigate on the improvement in their ZT values, especially high ZT values at high temperature to spread their applications at high-temperature operations.

Structural characteristics (including crystal structure, vacancy and antisite defects) and synthetic processes are essential factors affecting thermoelectric performance of Bi$_2$Te$_3$-based thermoelectric materials. For example, Bi$_2$Te$_3$-based compounds have anisotropic structure and resultant anisotropic electrical as well as thermal properties, which are desirable to modulate their thermoelectric performance. In addition, Bi$_2$Te$_3$-based compounds belong to layered narrow-band-gap semiconductors, which means they have good electrical conductivity but low thermal conductivity. Furthermore, synthesis processes can control the morphology and chemical composition of Bi$_2$Te$_3$-based compounds, which has great impact on their thermoelectric performance. Therefore, it is important and necessary to well understand their

structural characteristics and study synthesis processes before suggesting any strategies to improve their thermoelectric performance. However, there is no comprehensive summary or critical review on the advances of their structural characteristics and thermoelectric performance within the last decade. Thus, this review will present a comprehensive summary of the development of Bi_2Te_3-based thermoelectric materials within the last 10 years, identify challenges, and suggest some possible new opportunities.

1.2. Aims

This thesis project aims to comprehensively and critically study and review:

(1) the structural characteristics of Bi_2Te_3, $Bi_xSb_{2-x}Te_3$ and $Bi_2Te_{3-y}Se_y$, such as crystal structure, crystal parameters, band gap, vacancy and antisite defects;

(2) the relationships between their structural characteristics and thermoelectric performance;

(3) various synthesis processes used to manufacture bulk, thin-film and nanostructured Bi_2Te_3, $Bi_xSb_{2-x}Te_3$ and $Bi_2Te_{3-y}Se_y$ thermoelectric materials;

(4) the intrinsic thermoelectric properties and performance of Bi_2Te_3, $Bi_xSb_{2-x}Te_3$ and $Bi_2Te_{3-y}Se_y$;

(5) and approaches to improving their thermoelectric performance including how to maximize their electrical properties and how to minimize their thermal conductivity.

Finally, current challenges, possible research opportunities and some recommendations will be presented in the conclusion section.

1.3. Project Overview

To successfully complete this literature review on time, all the necessary work is divided into three periods. The detailed schedule of this thesis project is as follow:

- Semester 1 (27/02/2017 – 02/06/2017):

(1) Self-study and weekly discussion with my supervisors were conducted to gain understanding on fundamental principles in thermoelectrics to start this thesis project;

(2) Meeting with my supervisors was conducted to refine a reasonable and practical topic for my thesis;

(3) A rough thesis proposal was drafted at the start of this semester in order to determine the detailed objectives, structure and schedule of this thesis project;

(4) The main part of literature review on structural characteristics of Bi_2Te_3-based thermoelectric materials was completed;

(5) A small part of literature review on synthesis processes and strategies to enhance performance of Bi_2Te_3-based thermoelectric materials was completed;

(6) In order to have a deep insight into my thesis topic, frequent meeting with PhD colleagues in this field was made;

(7) In order to write a logical and systematical literature review, plenty of journal articles were studied;

(8) Risk management for this thesis project was completed (shown in Table 1);

(9) Frequent attendance to workshops was made to understand thesis requirements as well as have some useful advice.

- Winter Holiday (26/06/2017 – 23/07/2017):

(1) Refinement and reflection on what had been done in Semester 1 were performed;

(2) Comprehensive literature review on synthesis processes of Bi_2Te_3-based thermoelectric materials and comparison between these processes were completed.

- Semester 2 (24/07/2017 – 27/10/2017):

(1) Comprehensive literature review on intrinsic thermoelectric properties of Bi_2Te_3-based compounds and strategies to enhance their thermoelectric performance were completed;

(2) Weekly meeting with my supervisors and PhD colleagues in this field was conducted because of their expertise and supportive advice;

(3) Frequent attendance to workshops was made to understand thesis requirements as well as

have some useful advice;

(4) Current challenges were summarized and some recommendations on future research work were made;

(5) Final report was modified.

Table 1. Risk management for this thesis project.

Risk Identification	Consequences Caused	Likelihood	Seriousness	Risk Mitigation
Inadequate and non-comprehensive work before deadline	Reduced project output quality	Low	High	Re-modification of detailed timetable to reduce its likelihood during the whole thesis project
Inadequate access to necessary literature	Reduced project output quality	Medium	Medium	Approaching literature resources out of university libraries to reduced its likelihood and consultation with supervisors to reduce its seriousness during the whole thesis project
Misunderstanding of specific terminologies	Reduced project output quality	Low	High	Consultation with supervisors to reduce its likelihood and seriousness once the problem occurs
Lack of logicality in thesis	Reduced project output quality as well as extended timeframe	Medium	High	Weekly meeting with supervisors to reduce its likelihood during the whole thesis project

1.4.   Final Report Layout

The final report is composed of five chapters:

(1) Chapter 1 – Introduction

Chapter 1 intends to familiarize the background of thermoelectrics as well as fundamental information on this thesis project, and define the topic of this thesis. The background knowledge

also identifies the motivation behind this literature review – comprehensively and critically summarizing the advances of Bi_2Te_3-based thermoelectric materials within the last decade (including their structural characteristics, manufacturing processes and strategies to enhance thermoelectric performance). In addition, this chapter details the objectives as well as schedule of this thesis project and the layout of the final paper.

(2) Chapter 2 – Structural Characteristics of Bi_2Te_3-Based Thermoelectric Materials

Chapter 2 aims to overview the detailed structural characteristics of thermoelectric materials Bi_2Te_3, $Bi_xSb_{2-x}Te_3$, and $Bi_2Te_{3-y}Se_y$, such as crystal structure, crystal parameters, chemical bonding, band gap, vacancy and antisite defects, and the relationships between their structural characteristics and their thermoelectric properties. Chapter 2 also reviews the relationships between Sb content and properties of Bi_2Te_3-based materials as well as those between Se content and properties of Bi_2Te_3-based materials.

(3) Chapter 3 – Synthesis Processes of Bi_2Te_3-Based Thermoelectric Materials

Chapter 3 aims to comprehensively overview various manufacturing processes used to synthesize various bulk, thin-film and nanostructured Bi_2Te_3-Based thermoelectric materials, such as solvothermal/hydrothermal method, physical and chemical deposition (magnetron sputtering, thermal evaporation, flash evaporation and electrochemical deposition) and high-energy ball milling. Importantly, how synthesis processes affect the thermoelectric properties of Bi_2Te_3-Based materials has been reviewed. Then, this chapter makes a comparison between these processes, presents current challenges and suggests some potential recommendations on synthesis processes.

(4) Chapter 4 – Thermoelectric Performance Improvement of Bi_2Te_3-Based Thermoelectric Materials

Chapter 4 aims to firstly overview and study the underlying theory of improving thermoelectric performance of Bi_2Te_3-based materials. Then, based on increasing electrical conductivity, increasing Seebeck coefficient and suppressing thermal conductivity, various strategies to improve thermoelectric performance of Bi_2Te_3-based materials have been comprehensively reviewed and evaluated.

(5) Chapter 5 – Conclusion

Chapter 5 aims to summarize the main findings of this thesis, and then current challenges as well as possible opportunities are presented. Furthermore, some recommendations on future research work are provided.

2. Structural Characteristics of Bi₂Te₃-Based Thermoelectric Materials

2.1. Bi₂Te₃

Bi₂Te₃ has a space group of $D_{3d}^5 (R3m)$ and a rhombohedral crystal structure, which is also described as hexagonal unit cell.[15] Figure 2 exhibits the conceptual model of its hexagonal crystal structure. This hexagonal crystal structure consists of three lamellae, and there are five atoms within each lamella, which are stacked based on the sequence of $Te^{(1)} – Bi – Te^{(2)} – Bi – Te^{(1)}$. $Te^{(1)}$ and $Te^{(2)}$ refer to Te atoms with two different surroundings which are bonded with their nearest Bi atoms by different chemical bonds. Each single lamella is called as one quintuple layer (QL). The relationship between the determination of these planes and the trigonal axis (c-axis) is perpendicular. Therefore, Bi₂Te₃ has a layered structure.
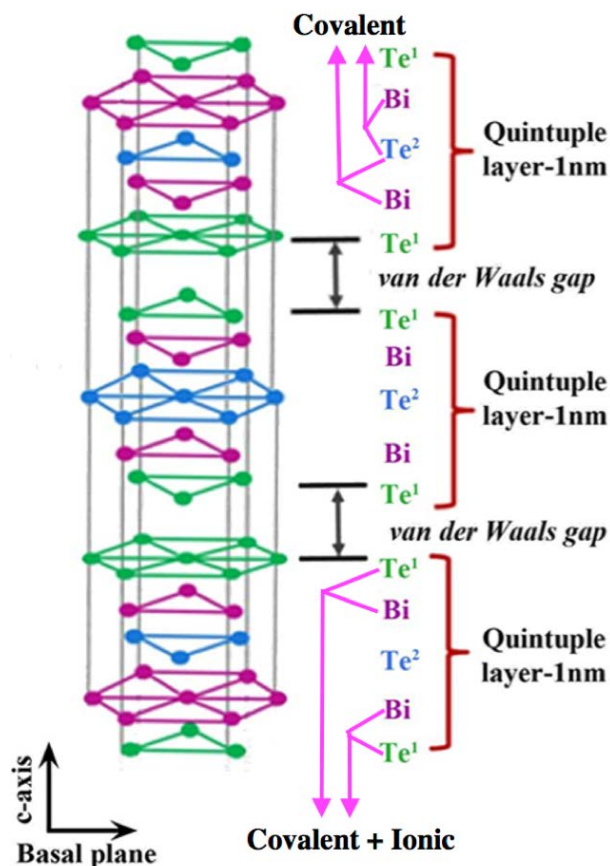
Figure 2. Crystal structure and bonding model of Bi₂Te₃.[16,17]

There are various chemical bonds within Bi_2Te_3 and Figure 2 shows its conceptual model of chemical bonding. Within one single lamella, $Te^{(1)} - Bi$ exhibits a bond length of 0.1 Å, whereas the bond length of $Te^{(2)} - Bi$ is a bit longer,[16,18] which indicates they are bonded by different types of chemical bonds. Indeed, the chemical bond between $Te^{(1)}$ and Bi atoms is a combination of covalent and ionic bonds, meanwhile $Te^{(2)}$ and Bi are only held together by covalent bond. However, $Te^{(1)}$ and $Te^{(2)}$ or $Te^{(1)}$ and $Te^{(1)}$ are connected by van der Waals interaction which is much weaker than the ionic-covalent bonding within the QL. Thus, bismuth telluride's structure and thermoelectric properties tend to be remarkably anisotropic due to its layered structure and the breakdown of week van der Waals bonds. For instance, cross-plane and in-plane lattice thermal conductivity for single crystalline Bi_2Te_3 is different (0.7 $Wm^{-1}K^{-1}$ and 1.5 $Wm^{-1}K^{-1}$ at 300 K respectively).[19] Moreover, single crystalline Bi_2Te_3 also shows anisotropy in electrical conductivity.[20]

An explanation of the anisotropy in Bi_2Te_3 can help to understand the enhancement of its thermoelectric efficiency. In fact, the degree of c-axis orientation has significant influence on in-plane (perpendicular to c axis) and cross-plane (parallel to c axis) electrical conductivity (σ) and Seebeck coefficient (S) of Bi_2Te_3 due to its anisotropy. The degree of c-axis orientation is described by Lotgering Factor that is calculated using Eqs.(3), (4) and (5):

$$F = \frac{P - P_0}{1 - P_0},$$
(3)

$$P_0 = \frac{\sum I_0(0\ 0\ l)}{\sum I_0(h\ k\ l)},$$
(4)

$$P = \frac{\sum I(0\ 0\ l)}{\sum I(h\ k\ l)},$$
(5)

where I_0 and I refer to the intensities of the diffraction peaks in the X-ray diffraction (XRD) analyses provided in the JCPDS file (15-0863) and those measured in laboratory experiment.[19] Table 2 and Figure 3 reveal how F value affects in-plane and cross-plane σ and S of single- and poly-crystalline Bi_2Te_3. It can be evidentially seen that in-plane normalized values of σ and S of Bi_2Te_3 increase with F value, but cross-plane normalized values of σ and S of Bi_2Te_3 decrease with F value. In particular, when $F = 0$, normalized values of in-plane and cross-plane σ and S are 1.0, which means in-plane and cross-plane σ and S are the same. However, when $F = 1.0$

Table 2. In-plane and cross-plane electrical conductivity and Seebeck coefficient of single- and poly-crystalline bulk Bi_2Te_3.[19]

Crystal Structure Bi_2Te_3	Single-Crystalline					Poly-Crystalline				
F Value	1.0		1.0		1.0	0.50		0.56		
	σ S/cm	S μV/K	σ S/cm	S μV/K	σ S/cm	σ S/cm	S μV/K	σ S/cm	S μV/K	
A In Plane (Perpendicular to c-Axis)	1000	-240	813	-228	660	855	-198	1087	-194	
B Cross Plane (Parallel to c-Axis)	185	-240	224	-206	150	480	-194	435	-191	
C Average (2A+B)/3	728	-240	617	-221	490	730	-197	870	-193	
A/C Normalized	1.37	1.00	1.32	1.03	1.35	1.17	1.01	1.25	1.01	
B/C Normalized	0.25	1.00	0.36	0.93	0.31	0.66	0.98	0.50	0.99	
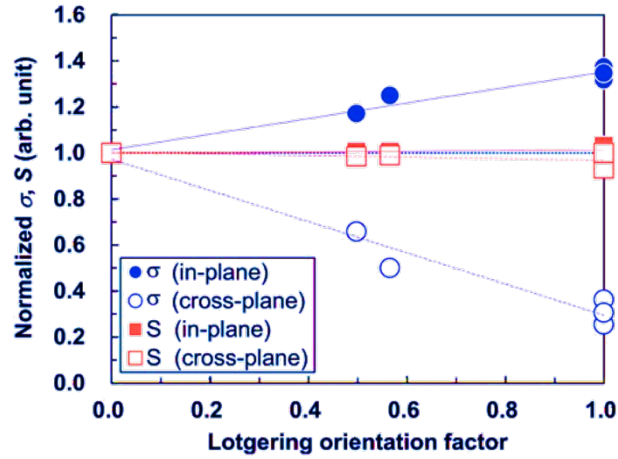
Figure 3. Plot of in-plane and cross-plane normalized electrical conductivity and Seebeck coefficient of bulk Bi_2Te_3 vs. F value.[19]

(highly c-axis oriented), in-plane σ and S are the highest but cross-plane σ and S are the lowest. In addition, it can be clearly noticed that anisotropy has more effects on σ than S. Thus,

anisotropy of Bi_2Te_3 can be employed to control its thermoelectric properties in different directions.

Table 3 summarizes the different lattice constants of Bi_2Te_3 that were reported by different literature. But, these lattice constants can be considered to be in agreement as they are very close to each other.

Table 3. A summary of lattice constants of Bi_2Te_3.

| | Lattice Constants | | Reference |
	a (Å)	c(Å)	
Bi_2Te_3	4.386	30.497	21
Bi_2Te_3	4.384	30.495	16
Bi_2Te_3	4.3835	30.487	22
Bi_2Te_3	4.440	31.998	23
Bi_2Te_3	4.327	31.357	23
Bi_2Te_3	4.409	30.778	23
Bi_2Te_3	4.443	31.153	23
Bi_2Te_3	4.463	31.741	23
Bi_2Te_3	4.610	32.477	23
Bi_2Te_3	4.36	30.38	18
Bi_2Te_3	4.37	30.51	18

Bi_2Te_3 consists of heavy elements which are bonded covalently. In addition, it exhibits a small band gap (shown in Table 4), and thus, it is a narrow-band-gap semiconductor.[6,24,25] Covalent bonding and narrow band gap tend to increase electron entropy and mobility. As a result, its narrow band gap and covalent bonding enable it to have high electrical conductivity, meanwhile its layered structure allows it to have low thermal conductivity, which encourages it to be a potential candidate for good thermoelectric materials.

Table 4. A summary of band gap of Bi_2Te_3.

	Band Gap (eV)	Reference
Bi_2Te_3	0.162	26
Bi_2Te_3	0.154	27
Bi_2Te_3	0.165	23
Bi_2Te_3	0.157	23
Bi_2Te_3	0.170	23
Bi_2Te_3	0.156	23
Bi_2Te_3	0.13	18

2.2. $Bi_xSb_{2-x}Te_3$

Sb_2Te_3 shares the same space group of $D_{3d}^5(R3m)$ and the same rhombohedral crystal structure with Bi_2Te_3.[13] It also shares a similar electronic structure with Bi_2Te_3. Table 5 summarizes the lattice constants of Sb_2Te_3 reported in different journal articles and it can be noticed that the lattice constants of Sb_2Te_3 are slightly smaller than Bi_2Te_3 because Sb possesses a slightly smaller atomic radius than Bi.

Table 5. A summary of lattice constants of Sb_2Te_3.

| | **Lattice Constants** | | **Reference** |
	a (Å)	*c*(Å)	
Sb_2Te_3	4.264	30.458	28
Sb_2Te_3	4.44	30.29	29
Sb_2Te_3	4.25	30.4	29

Since Sb_2Te_3 can completely dissolve in Bi_2Te_3 to form solid solutions in any proportion and possesses a structure similar to Bi_2Te_3, $Bi_xSb_{2-x}Te_3$ shows the same crystal structure as Bi_2Te_3. $Bi_xSb_{2-x}Te_3$ is layer-structured and it is a repetition of $Te^{(1)}$ – Bi (or Sb) – $Te^{(2)}$ – Bi (or Sb) – $Te^{(1)}$ lamellae. The lamellae within $Bi_xSb_{2-x}Te_3$ are connected by van der Waals bonds, which are weaker than bonds between Te and Bi (or Sb).

The difference between chemical bonds within $Bi_xSb_{2-x}Te_3$ leads to the volatilization of $Te^{(1)}$, especially at high temperature, and to consequent Te vacancy, $V_{Te}^{\cdot\cdot}$. However, Bi or Sb atoms can easily occupy this type of Te vacancy because these three atoms have a similar electronegativity.[30] This occupation results in antisite defect Bi'_{Te} or Sb'_{Te}, new vacancy V_{Bi}''' and V_{Sb}''' as well as increased concentration of hole $h^{\cdot}$. As a result, antisite defects can be used to tune electrical conductivity of Bi_2Te_3-based solid solutions. These antisite defects are hardly to detect through energy-dispersive X-ray spectroscopy (EDS) because of their relatively low concentration, but they can be evidentially proved by the measurement of lattice parameters and cell volumes because Bi and Sb have a radius of 1.6 Å and 1.45 Å respectively, but Te has a radius of only 1.40 Å.[31] For instance, lattice parameters and cell volume of $Bi_{0.5}Sb_{1.5}Te_3$ increase with hydrogen annealing temperature (shown in Table 6) because of the volatilization

of Te atoms, which indicates antisite defects Bi'_{Te} and/or Sb'_{Te}, and new vacancy V'''_{Bi} and/or V'''_{Sb} produced.

Table 6. Lattice constants and cell volumes of $Bi_{0.5}Sb_{1.5}Te_3$.[32]

Sample	H₂ Annealing Temperature (K)	Lattice Constant (Å)		Cell Volume (Å³)
		a-Axis	c-Axis	
Unannealed	-	4.2928	30.4093	485.3090
	523	4.2930	30.4152	485.4484
H₂-Annealed	673	4.2968	30.4518	486.8934
	823	4.2970	30.4860	487.4856

2.3. Bi₂Te₃₋ySey

Like Sb_2Te_3, Bi_2Se_3 shares the same space group of $D_{3d}^5 (R3m)$ and the same rhombohedral crystal structure with Bi_2Te_3. It also shares a similar electronic structure with Bi_2Te_3. Since Bi_2Se_3 can completely dissolve in Bi_2Te_3 to form solid solutions in any proportion and possesses a structure similar to Bi_2Te_3, the formed solid solution $Bi_2Te_{3-y}Te_y$ shows the same crystal structure as Bi_2Te_3. $Bi_2Te_{3-y}Te_y$ is layer-structured and it is a repetition of $Te^{(1)}$ (or $Se^{(1)}$)– $Bi – Te^{(2)}$ (or $Se^{(2)}$)– $Bi – Te^{(1)}$ ($Se^{(1)}$) lamellae. The lamellae within $Bi_2Te_{3-y}Te_y$ are held together by van der Waals bonds which are much weaker than chemical bonds between Te (or Se) and Bi.

Table 7 summarizes lattice parameters of $Bi_2Te_{3-y}Se_y$, and Figure 4 plots the relationship between lattice parameters and composition $Bi_2Te_{3-y}Se_y$. It can be evidentially seen that the increased Se concentration results in the decreased lattice parameters a and c. This decrease is due to the smaller Se atoms as Te and Se possess an atomic radius of 1.4 Å and 1.15 Å respectively.[33] In addition, after Se atoms added, Se atoms occupies Te atoms within Bi_2Te_3. $Te^{(2)}$ atoms are initially replaced and then $Te^{(1)}$ atoms are replaced by Se atoms. This replacement leads to strengthened alloy scattering for electrons and phonons, which consequently results in suppressing carrier (electron) mobility and lattice thermal conductivity reduction. Therefore, thermoelectric performance of $Bi_2Te_{3-y}Se_y$ can be predicted to change with addition of different Se concentrations.

Table 7. Lattice parameters of $Bi_2Te_{3-y}Se_y$.[33]

Composition		Lattice Constant (Å)	
Nominal	Actual	a	c
Bi_2Te_3	$Bi_{2.02}Te_{2.92}$	4.383	30.414
$Bi_2Te_{2.85}Se_{0.15}$	$Bi_{1.96}Te_{2.89}Se_{0.15}$	4.368	30.362
$Bi_2Te_{2.7}Se_{0.3}$	$Bi_{1.98}Te_{2.73}Se_{0.29}$	4.345	30.344
$Bi_2Te_{2.55}Se_{0.45}$	$Bi_{1.99}Te_{2.58}Se_{0.43}$	4.336	30.266
$Bi_2Te_{2.4}Se_{0.6}$	$Bi_{1.94}Te_{2.35}Se_{0.61}$	4.323	30.111
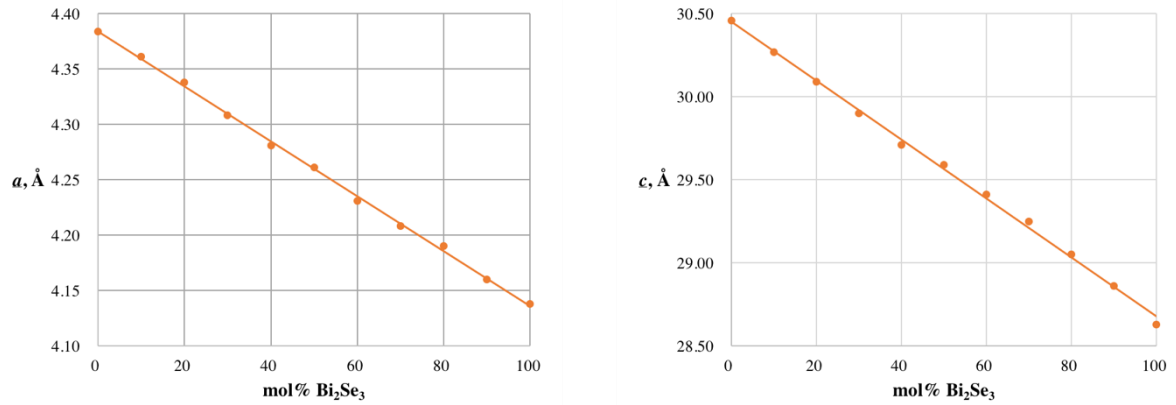
Figure 4. Plot of lattice parameters vs. Bi_2Se_3 concentration.[16]

Table 8. Electronic transport properties of $Bi_2Te_{3-y}Se_y$.[33]

Composition		Mobility $(cm^2V^{-1}s^{-1})$	Carrier Concentration (cm^{-3})
Nominal	Actual		
Bi_2Te_3	$Bi_{2.02}Te_{2.92}$	96.92	7.63×10^{19}
$Bi_2Te_{2.85}Se_{0.15}$	$Bi_{1.96}Te_{2.89}Se_{0.15}$	84.65	6.87×10^{19}
$Bi_2Te_{2.7}Se_{0.3}$	$Bi_{1.98}Te_{2.73}Se_{0.29}$	75.74	5.98×10^{19}
$Bi_2Te_{2.55}Se_{0.45}$	$Bi_{1.99}Te_{2.58}Se_{0.43}$	75.30	5.17×10^{19}
$Bi_2Te_{2.4}Se_{0.6}$	$Bi_{1.94}Te_{2.35}Se_{0.61}$	73.44	4.29×10^{19}

Electrical transport properties of $Bi_2Te_{3-y}Se_y$, such as carrier mobility and concentration, are highly affected by both antisite defects and anion vacancies. If γ, which is referred to the ratio of anion and cationic components, is smaller than 3/2, Te sites will be occupied by Bi atoms and consequently lead to Bi_{Te} antisite defects that serve as electron acceptors. By contrast, if γ is larger than 3/2, Bi sites will be occupied by Te atoms and consequently result in Te_{Bi} antisite defects that serve as electron donors. In $Bi_2Te_{3-y}Se_y$, if γ is smaller than 1.2, Te_{Bi} antisite defects will decrease with increasing Se concentration, which leads to carrier concentration and

mobility reduction as electrons are major carriers in $Bi_2Te_{3-y}Se_y$ (shown in Table 8). As a result, electrical conductivity that is determined by carrier concentration and mobility is reduced with the increment of Se content.

3. Synthetic Processes of Bi$_2$Te$_3$-Based Thermoelectric Materials

Bi$_2$Te$_3$-based thermoelectric materials represent an important part of thermoelectric materials because this category of thermoelectric materials exhibits high *ZT* near temperature range 200-400 K,[11,12] which allows its application in power generation at room temperature. Extensive research has been conducted to investigate various synthesis processes of Bi$_2$Te$_3$-based thermoelectric materials. To date, many synthesis methods have been studied and applied, and these methods show themselves advantages and disadvantages. Therefore, it is important to comprehensively and critically review and compare these methods in order to understand how to fabricate Bi$_2$Te$_3$-based thermoelectric materials with high efficiency. This section will comprehensively review the progress in their synthesis processes within the last decade. Actually, Bi$_2$Te$_3$-based thermoelectric materials can be fabricated by various processes, and traditional ones include solvothermal/hydrothermal method, physical and chemical deposition (magnetron sputtering, thermal evaporation, flash evaporation and electrochemical deposition) and high-energy ball milling. Appendix A summarizes and Appendix B compares different synthesis processes used to fabricate Bi$_2$Te$_3$-based thermoelectric materials. For every single synthesis process, some recommendations will be made.

3.1. Solvothermal/Hydrothermal Method

Up to date, many synthesis processes have been applied to fabricate nanostructured Bi$_2$Te$_3$-based thermoelectric materials due to their high thermoelectric performance. Compared with other processes, such as electrochemical deposition and transformation from nanoparticles using thermal processes, solvothermal/hydrothermal method is much simpler to fabricate nanostructured Bi$_2$Te$_3$-based thermoelectric materials with different morphology and sizes due to its one-step reaction.[34,35] In addition, solvothermal/hydrothermal synthesis is very cost-efficiency. As a result, these benefits enable this method to become the most common process to fabricate one-dimensional Bi$_2$Te$_3$-based thermoelectric materials. For instance, Song et al. reported the successful fabrication of Bi$_2$Te$_3$ nanorod grown by solvothermal method.[36] Solvothermal and hydrothermal methods are very similar in operation and essence, and the only

difference between them is the type of precursor solutions. If the precursor solutions are non-aqueous, the synthesis process is hydrothermal; meanwhile if the precursor solutions are aqueous, the synthesis process is solvothermal. This section aims to review and evaluate Bi_2Te_3-based nanostructures with different morphology and sizes which are formed by solvothermal method, and also aims to offer some recommendations on this synthetic method.

Serrate-like Bi_2Te_3 nanostructures can be produced through solvothermal synthesis, which follows a typical process: preparation of precursor solution, high-temperature reaction in an autoclave, cooing and collection.[37] $Bi(NO_3)_3 \cdot 5H_2O$ forms homogeneous solution in deionized water, and Na_2TeO_3 is then added into this solution, resulting in precipitate of $Bi_2(TeO_3)_3$. The mixture of solution and precipitate is then stirred for 10 minutes, after which ascorbic acid, polyvinyl pyrrolidone, and ethylene glycol are added simultaneously. The newly formed solution is stirred again for 20 minutes and a suspension is then formed. The suspension (precursor solution) is transported into a Teflon-lined stainless steel autoclave and heated at 473 K for 24 hours, after which the autoclave is cooled to room temperature in the open space. The black product is collected, which needs to experience centrifugation and three-time wash with deionized water and pure ethanol in order to collect the target product (Bi_2Te_3 nanostructures). Eventually, the washed product is dried in vacuum at 333 K. All starting chemicals are purchased and used directly without any further purification.

In the solvothermal synthesis of serrate-like nanostructured Bi_2Te_3 performed by Jiang et al.,[37] the formation of target product is accompanied with impurities and its morphology is not so satisfying, although this synthesis process is very simple. This is attributed to the insufficient chemical reaction rate during solvothermal process. The chemical reaction rate greatly affects the purity and surface topology of the synthesized Bi_2Te_3. For Bi_2Te_3 fabricated through solvothermal method, the chemical reaction with adequate reaction rate can proceed quickly to the final stage to produce the target product, meanwhile the reaction with inadequate reaction rate may terminate at any intermediate stage to produce impurities. Since the chemical reaction rate is very important to the purity and morphology of the target product, enhancing the reaction rate during synthesis is required. Actually, solvothermal method means synthesis at high temperature which is helpful to accelerate the synthesis reaction, but it is not enough. Takashiri

et al. reported that both stirring before and during synthesis reaction at high temperature are useful to improve reaction rate and consequently, nanostructured Bi_2Te_3 with perfect morphology and high quality is collected.[38] This results from uniform temperature and concentration in precursor solution which is due to the constant stirring during reaction. Furthermore, constant stirring during solvothermal synthesis contributes to reducing the time requirement, which is favourable from industrial perspective.
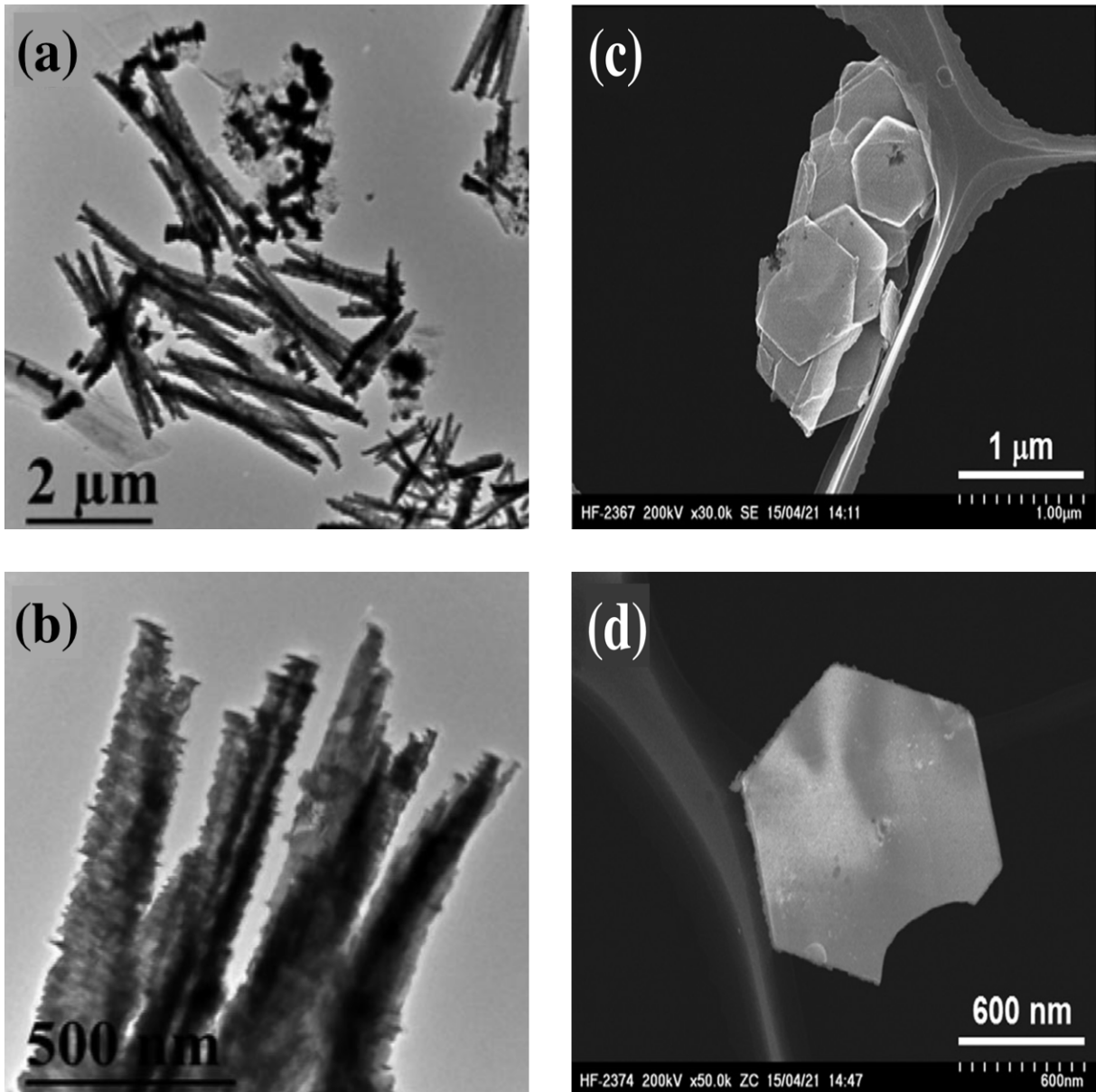
Figure 5. Comparison of morphology of nanostructured Bi_2Te_3 synthesized by solvothermal process without (a-b) and with (c-d) stirring during reaction at high temperature.[37,38]

In addition to the high purity resulting from stirring-assisted solvothermal method, nanostructured Bi_2Te_3 fabricated from solvothermal synthesis without and with stirring also

exhibit different morphology (shown in Fig. 5): serrate-like nanostructures and nanoplates respectively. Compared with serrate-like nanostructures, nanoplates are more favourable from thermoelectric perspective because nanoplates possess many features which have great effect on enhancing the performance of thermoelectric materials. For instance, high crystallinity contributes to high electrical conductivity, well-defined atomic ratio contributes to improvement in Seebeck coefficient, and ultra-low thickness of nanoplates contributes to increased phonon scattering and consequent low thermal conductivity.

Solvothermal method is often applied to fabricate nanostructured Bi_2Te_3-based thermoelectric materials, such as one-dimensional nanostructures (nanowires and nanotubes),[39-41] two-dimensional nanostructures (nanoplates) and three-dimensional nanostructures (spindly structures and flower-like nanostructures). Compared with other nanostructures (like serrate-like nanostructures and nanoplates), three-dimensional hierarchitectures (such as flower-like Bi_2Te_3) exhibits excellent thermoelectric properties. For instance, flower-like Bi_2Te_3 has a higher value of electric conductivity than Bi_2Te_3 nanoparticles, and resultant higher power factor and higher ZT.[42] This results from smaller density of grain boundaries and consequent suppressed carrier scattering at grain boundaries.[43] Furthermore, the smaller density of grain boundaries originates from the thick nanoplates (30 nm in thickness) which flower-like Bi_2Te_3 is composed of.

Jin et al. reported the successful formation of flower-like nanostructured Bi_2Te_3 by using solvothermal method.[42] Their synthesis follows a typical solvothermal process: preparation of precursor solution, high-temperature synthetic reaction in an autoclave, cooling and collection. Their precursor solution consists of $Bi(NO_3)_3 \cdot 5H_2O$, Na_2TeO_3, ethylene glycol, glucose, NaOH and $N_2H_4 \cdot H_2O$. The formed precursor solution is then transported into a Teflon-lined stainless-steel autoclave and heated at 453 K for 8 hours. Finally, the flower-like nanostructured Bi_2Te_3 is cooled, washed and dried. SEM images show that the synthesized Bi_2Te_3 has a flower-like morphology which is 300-2000 nm in width. These flower-like nanostructured Bi_2Te_3 is made from nanoplates which is 30 nm in thickness.

The formation of flower-like nanostructured Bi_2Te_3 is controlled by three factors: the amount of glucose, the NaOH concentration and the growth temperature.[42] In the growth of flower-like
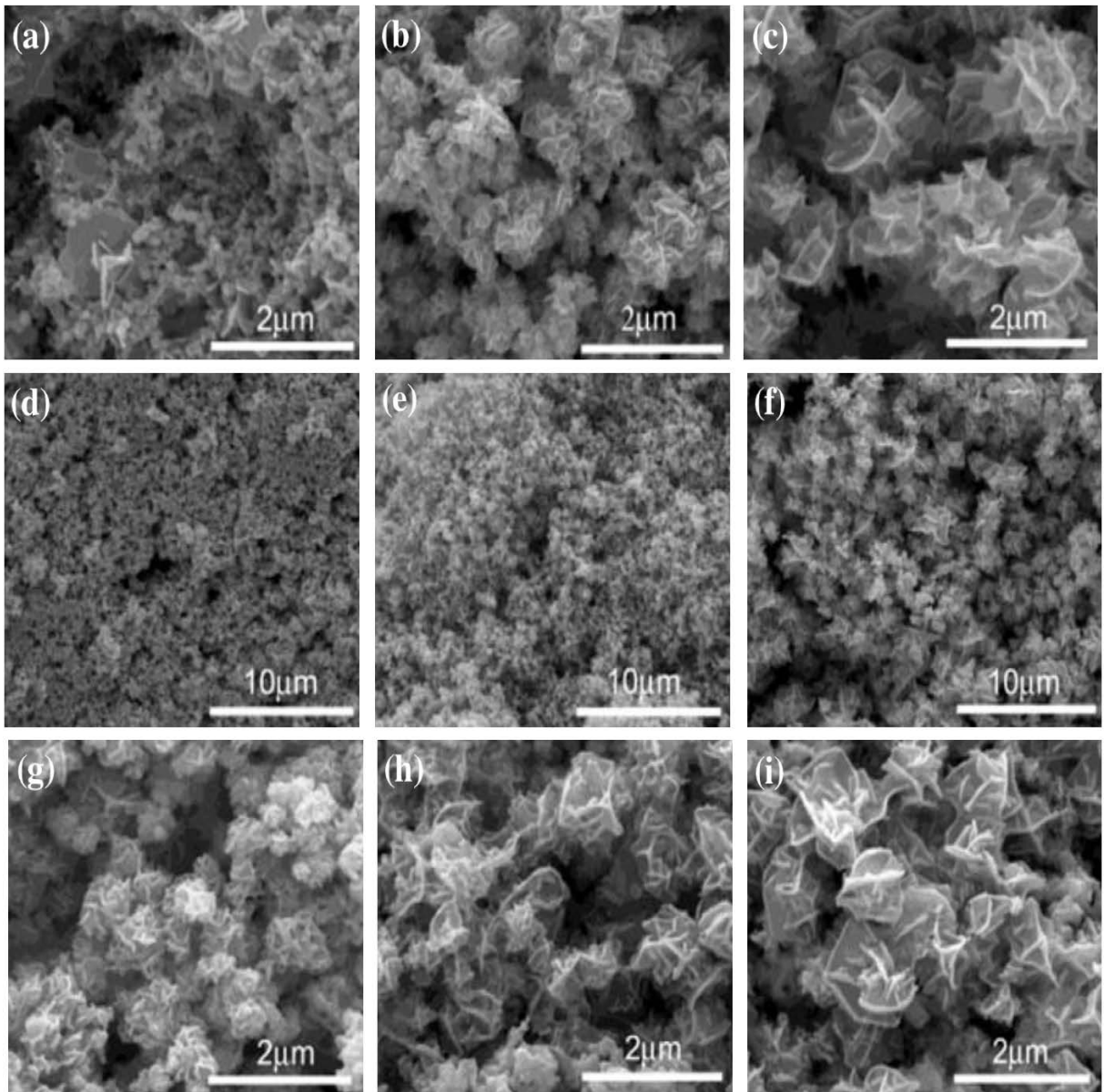
Figure 6. Comparison of morphology of nanostructured Bi_2Te_3 prepared with different amount of glucose: (a) 0 g, (b) 0.4 g, (c) 0.8 g; with different NaOH concentration: (d) 0 g, (e) 0.1 g, (f) 0.3 g; at different growth temperature: (g) 393 K, (h) 433 K, and (i) 473 K.[42]

nanostructured Bi_2Te_3, glucose serves as an assembled stimulative reagent, which can promote Bi_2Te_3 to aggregate in order to form microspheres and the final flower-like nanostructured Bi_2Te_3. With increasing amount of glucose used in the fabrication process, the aggregation effect becomes more noticeable, which results in more flower-like nanostructured Bi_2Te_3 fabricated (shown in Fig. 6(a-c)). Like glucose, NaOH concentration also has great effect on the formation of flower-like Bi_2Te_3. Theoretically, the addition of NaOH contributes to the anisotropic growth of Bi_2Te_3. This means that the formation of flower-like nanostructured

Bi$_2$Te$_3$ increases with the NaOH concentration (shown in Fig. 6(d-f)). Furthermore, growth temperature makes important contribution to the formation of flower-like nanostructured Bi$_2$Te$_3$. Higher growth temperature enhances the aggregation process and the anisotropic growth. As a result, as growth temperature increases, the formation of flower-like nanostructured Bi$_2$Te$_3$ increases, meanwhile the Bi$_2$Te$_3$ nanoparticles decreases (shown in Fig. 6(g-i)).

To summarize, solvothermal/hydrothermal method is an important and universal process used to produce nanostructured Bi$_2$Te$_3$-based thermoelectric materials with different sizes and morphology, and this method follows a typical and simple process: preparation of precursor solution, high-temperature synthetic reaction, cooling and collection. Constant stirring during high-temperature synthetic reaction contributes to increased chemical reaction rate and resultant increased phase purity, meanwhile the use of glucose and NaOH is useful to control the morphology of nanostructured Bi$_2$Te$_3$-based thermoelectric materials. Since the phase purity and morphology have great effect on the quality of nanostructured Bi$_2$Te$_3$-based thermoelectric materials, more research work should be conducted on how to enhance the chemical reaction rate (such as possible use of catalyzers and increasing precursor concentration) as well as how to identify and fabricate the desired morphology.

3.2. Physical and Chemical Deposition

3.2.1. Magnetron Sputtering

Thin films of Bi$_2$Te$_3$ and its derivatives have been extensively investigated due to their high thermoelectric performance, and many synthesis technologies can be applied to prepare these thin films, including molecular beam epitaxy and normal sputtering. Compared with these technologies, magnetron sputtering which is an advanced sputtering technology is extensively employed to prepare large-scale thin films because magnetron sputtering does not require complex starting materials and it is cost-efficiency. For instance, Sb$_2$Te$_3$ thin films with a high power factor have been successfully deposited onto Si substrates through this method.[44] Magnetron sputtering includes radio frequency (RF) and direct current (DC) magnetron sputtering. RF and DC magnetron sputtering are very similar and they are powered by radio

frequency and direct current respectively.[45,46] This section aims to review and evaluate Bi_2Te_3-based thin films fabricated by magnetron sputtering, and intends to provide some suggestions on this synthesis method.

Kusagaya et al. have announced the successful application of RF magnetron sputtering in preparing nanocrystalline Bi_2Te_3 thin films.[47] During their synthesis process, dense and high-quality alloy Bi_2Te_3 serves as the sputtering target. Kapton substrates are firstly selected and their temperature is maintained at 473 K. In addition, substrates are evolved at 20 rpm, which helps to fabricate homogeneous Bi_2Te_3 thin films. The sputtering target is 140 mm far from substrates. Before the fabrication process, the chamber is vacuumed to 2.5×10^{-4} Pa. The deposition process is performed in 1.0 Pa of argon atmosphere and is powered by 200 W of radio frequency, which lasts for 1 hour. Eventually, 0.7-μm nanocrystalline Bi_2Te_3 thin films were successfully fabricated. Kusagaya and Takashiri have also conducted similar experimental work and successfully prepare high-quality nanocrystalline Bi_2Te_3 and Sb_2Te_3 thin films through RF magnetron sputtering.[48] In addition, a similar RF magnetron sputtering process has been implemented to manufacture $Bi_{0.5}Sb_{1.5}Te_3$ thin films.[49]
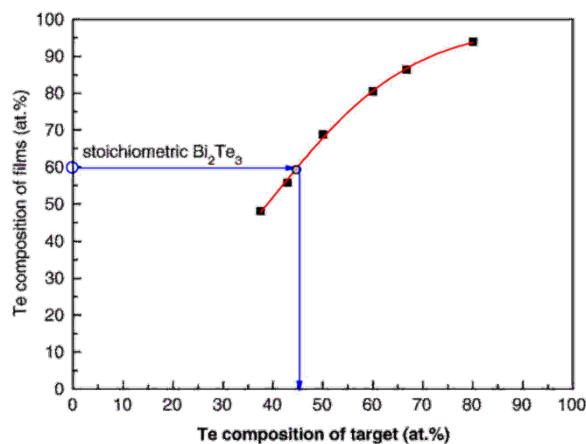
Figure 7. Te composition of sputtering target vs. Te composition of deposited films.[46]

However, the substrate is suggested to remain cool by flowing water during the sputtering process because high temperature of the substrate results in re-evaporation of Bi and Te. The substrate should be rotated continuously in order to achieve homogeneous thin films. In addition, low sputtering energy should be selected to avoid the Bi and Te powers scattering. Furthermore, due to the different sputtering rates of Bi and Te, it is challenging to fabricate

Bi$_2$Te$_3$ thin films with accurate atomic composition.[49] When the same sputtering energy is applied, it is easier for Te to be sputtered because Te possesses a lower thermal evaporation than Bi (52.5 kJ/mol and 104.8 kJ/mol respectively).[46] The relationship between Te concentration of deposited Bi$_2$Te$_3$ films and the Te concentration of sputtering target is illustrated in Fig. 7. Bi$_2$Te$_3$ thin films with 60 at.% Te can be deposited with 45 at.% Te in the sputtering target. Thus, the mixture powers of Bi and Te rather than bulk alloy Bi$_2$Te$_3$, and the use of magnetron sputtering help to produce stoichiometric Bi$_2$Te$_3$ films.

Huang et al. have reported the successful fabrication of Bi$_2$Te$_3$ thin films with accurate atomic ratio through RF magnetron sputtering.[46] The mixture powers of Bi and Te with high purity serve as the starting materials (sputtering target), which are put onto a non-magnetic disk. Amorphous structure quartz glass serves as the substrate, which is washed by formaldehyde, deionized water and pure alcohol respectively. The substrate remains cool by flowing water during the sputtering process and is revolved at 30 rpm. Before sputtering, the chamber is vacuumed to 1×10^{-3} Pa. The magnetron sputtering is powered by a small intensity of about 1 W/cm^2. Finally, the as-deposited Bi$_2$Te$_3$ thin films are annealed below 573 K within N$_2$ atmosphere in order to crystallize. The eventually fabricated Bi$_2$Te$_3$ thin films with accurate atomic composition are 350 nm in thickness. The as-deposited Bi$_2$Te$_3$ thin films are amorphous due to the use of an un-heated and amorphous quartz substrate which cannot trigger the crystal growth of Bi$_2$Te$_3$. Meanwhile, after annealing, the crystallization of Bi$_2$Te$_3$ thin films appears, which is attributed to diffusion and agglomeration of Bi and Te atoms caused by the increasing annealing temperature.

Thermal annealing after RF magnetron sputtering results in crystallization of Bi$_2$Te$_3$ thin films, which consequently elevates their electrical conductivity caused by increased carrier mobility. Further elevating the thermoelectric efficiency of Bi$_2$Te$_3$ thin films can be realized by fabricating highly c-axis oriented thin films. As mentioned in Section 2.1, the anisotropy of Bi$_2$Te$_3$ and its derivatives can be used to tune their thermoelectric properties and consequently obtain high-performance Bi$_2$Te$_3$-based thermoelectric materials. Actually, electron beam (EB) irradiation can be implemented to produce highly c-axis oriented Bi$_2$Te$_3$ thin films. Therefore, the combination of RF magnetron sputtering, EB irradiation and thermal annealing can be used

to fabricate highly c-axis oriented nanocrystalline Bi_2Te_3 thin films because EB irradiation can improve the crystal orientation, meanwhile thermal annealing can enhance the high crystallinity of nanocrystalline structures.

For example, Yamauchi and Takashiri have reported the successful fabrication of highly c-axis oriented nanocrystalline Bi_2Te_3 thin films through RF magnetron sputtering combined with EB irradiation and thermal annealing.[19] In their experimental work, high-quality Bi-Te material serves as the sputtering target. Corning Eagle XG glass serves as the substrates, which are evolved at 20 rpm in order to produce homogeneous thin films. The distance between sputtering target and substrates is 140 mm. The sputtering process is operated within 1.0 Pa of argon atmosphere and is powered by 200 W of radio frequency. The as-deposited films experience EB irradiation in nitrogen atmosphere, followed by thermal annealing. Finally, the fabricated nanocrystalline Bi_2Te_3 thin films are highly c-axis oriented and are 300 ± 50 nm in thickness. Similar experimental work is conducted by Takashiri et al. and they also have successfully fabricated highly c-axis oriented nanocrystalline Bi_2Te_3 thin films through RF magnetron sputtering combined with EB irradiation and thermal annealing.[50] Figure 8 plots the crystal orientation (Lotgering Factor, F) vs. EB irradiation dose. Lotgering Factor is described as the degree of c-axis orientation and calculated by Eqs.(3), (4) and (5). It can be noticed that Lotgering Factor is hugely increased by EB irradiation, especially EB irradiation of $0.22 - 0.86$ MGy. This means that EB irradiation allows Bi_2Te_3 thin films to be highly c-axis oriented.
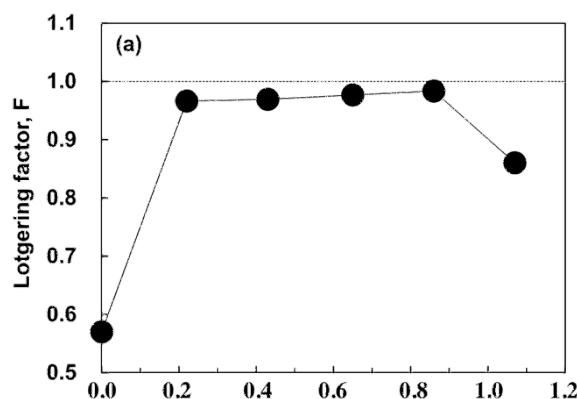
Figure 8. Plot of the crystal orientation (Lotgering Factor, *F*) vs. EB irradiation dose.[19]

To summarize, magnetron sputtering is a simple and cost-efficiency synthesis process to mainly fabricate Bi_2Te_3-based thin films. For the application of this synthesis method, several key

points should be considered: (1) the sputtering target should be composed of individual atom elements rather than bulk alloys in order to obtain thin films with accurate stoichiometry; (2) the selected substrates should be cooled by flowing water in order to avoid evaporation of atom elements; (3) the selected substrates should be rotated continuously to obtain homogeneous films; (4) low sputtering power should be implemented in order to avoid the atom element scattering; and (5) EB irradiation and thermal annealing, following sputtering, help to obtain Bi_2Te_3-based thin films with high thermoelectric efficiency. Furthermore, I suggest the use of appropriate substrates in the magnetron sputtering process, which can directly trigger the crystal growth of Bi_2Te_3-based thin films. This is because direct crystallization on cool substrates can be time-saving as well as energy-efficient. Thus, the future research work should attach emphasis on the types of substrates in order to identify substrates which can meet this requirement. Another possible research opportunity may be related to the distance between sputtering target and substrates. Morphology of Bi_2Te_3-based thin films has important influence on their thermoelectric properties and thus, the distance between sputtering target and substrates should be set to an appropriate value because the sputtering distance may affect the morphology.

3.2.2. Thermal Evaporation

Thin films have played an important role in thermoelectrics because they usually exhibit high thermoelectric performance and can be used to design portable thermoelectric devices, and thermal evaporation method is an attractive process to fabricate Bi_2Te_3-based thin films because this synthesis process is time-saving and does not require expensive facilities (low fabrication costs).

Thermal evaporation method has been adopted to prepare various thermoelectric thin films. For instance, Sb_2Te_3 thin films have been reported to be successfully fabricated by this method.[51] High-quality Sb_2Te_3 ingots are firstly ground into powers. The ground Sb_2Te_3 alloy powers serve as evaporation source, which are placed onto a tungsten boat. 60 A of current serves as the power to evaporate Sb_2Te_3 powers. SiO_2/Si serves as the substrates, and the temperature of substrates varies from room temperature to 423 K. Before evaporation, the chamber is vacuumed to 5.0×10^{-3} Pa. Under these experimental conditions, the consequent evaporation rate is approximately 16 Å/s. Substrate temperature has no impact on the thickness of Sb_2Te_3

thin films which is approximately 0.4 µm. Other literature has also reported the use of a similar thermal evaporation process to fabricate Bi_2Te_3 and Sb_2Te_3 thin films.[52,53]

Bi_2Te_3-based thin films with high crystallinity are favourable for thermoelectric applications because high crystallinity contributes to high electrical conductivity. The substrate temperature greatly affects the crystal structure of Sb_2Te_3 thin films prepared by thermal evaporation.[51] Figure 9 illustrates the dependence of crystalline properties of Sb_2Te_3 thin films on substrate temperature. Figure 9(b) shows that Sb_2Te_3 thin films deposited at room temperature are amorphous, which can be explained by the fact that Sb_2Te_3 does not have sufficient energy to diffuse, aggregate and crystallize at room temperature. When temperature rises, the peaks of Sb_2Te_3 thin films become stronger, which suggests the higher crystallinity. Interestingly, when temperature arrives at 423 K, (0 1 5) plane of Sb_2Te_3 shows the strongest peak (Fig. 9(g)), which indicates the highly c-axis oriented Sb_2Te_3 thin films. As a result, when thermal evaporation process is adopted to prepare thin films, an appropriate temperature should be maintained on the substrates in order to maximize the crystallinity and crystal orientation of thin films.
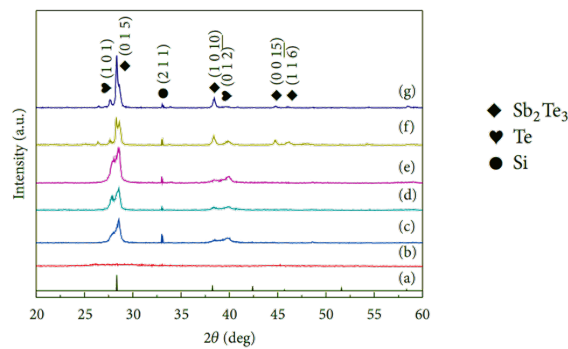
Figure 9. XRD patterns of Sb_2Te_3 thin films deposited by thermal evaporation at different temperatures: (a) JCPDS card; (b) room temperature; (c) 323 K; (d) 348 K; (e) 373 K; (f) 398 K; and (g) 423 K.[51]

To summarize, thermal evaporation process is a simple and time-saving method to produce Bi_2Te_3-based thin films, and the substrate temperature has great impact on the crystalline structure of films. However, few literature articles have reported the application of thermal evaporation in manufacturing Bi_2Te_3-based thin films. Thus, in the future, there should be more

research work conducted on how to ensure the accurate stoichiometry. The challenge of ensuring accurate stoichiometry may be met by using the mixture of elemental powers (mixed at a certain ratio) as the evaporation source. In addition, elemental nanopowers may be used as the evaporation source in order to fabricate nanocrystalline thin films that tend to exhibit high thermoelectric performance. Another possible research opportunity may be related to the control of morphology that can significantly affect thermoelectric properties of Bi_2Te_3-based thin films. Morphology may have association with both the distance between evaporation source and the tungsten boat and the evaporation rate determined by evaporation power. Therefore, future efforts should be made on investigating how the distance between evaporation source and the tungsten boat and the evaporation rate affect the morphology of Bi_2Te_3-based thin films and their resultant thermoelectric properties. Furthermore, slow evaporation rate can allow Bi_2Te_3-based thin films to have more time to crystallize and thus, the relationship between evaporation rate and crystallization of Bi_2Te_3-based thin films should be studied.

3.2.3. Flash Evaporation
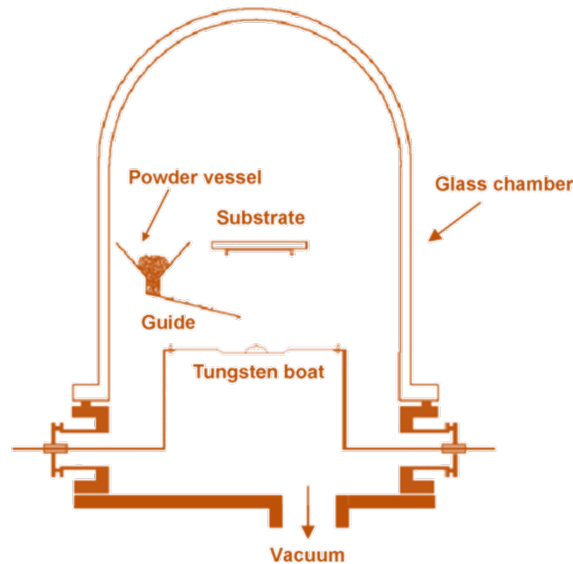
Figure 10. Conceptual model of flash evaporation system.[54]

Flash evaporation system is typically composed of power vessel, tungsten boat, substrate, vacuum and glass chamber (shown in Fig. 10). Like thermal evaporation, flash evaporation is mainly used to fabricate thin films, and the only difference between them is that evaporation source is continuously fed onto tungsten boat during flash evaporation while evaporation source

is directly put onto tungsten boat during thermal evaporation. In addition, it is the simple evaporation system that allows flash evaporation method to be simple and cost-efficiency.
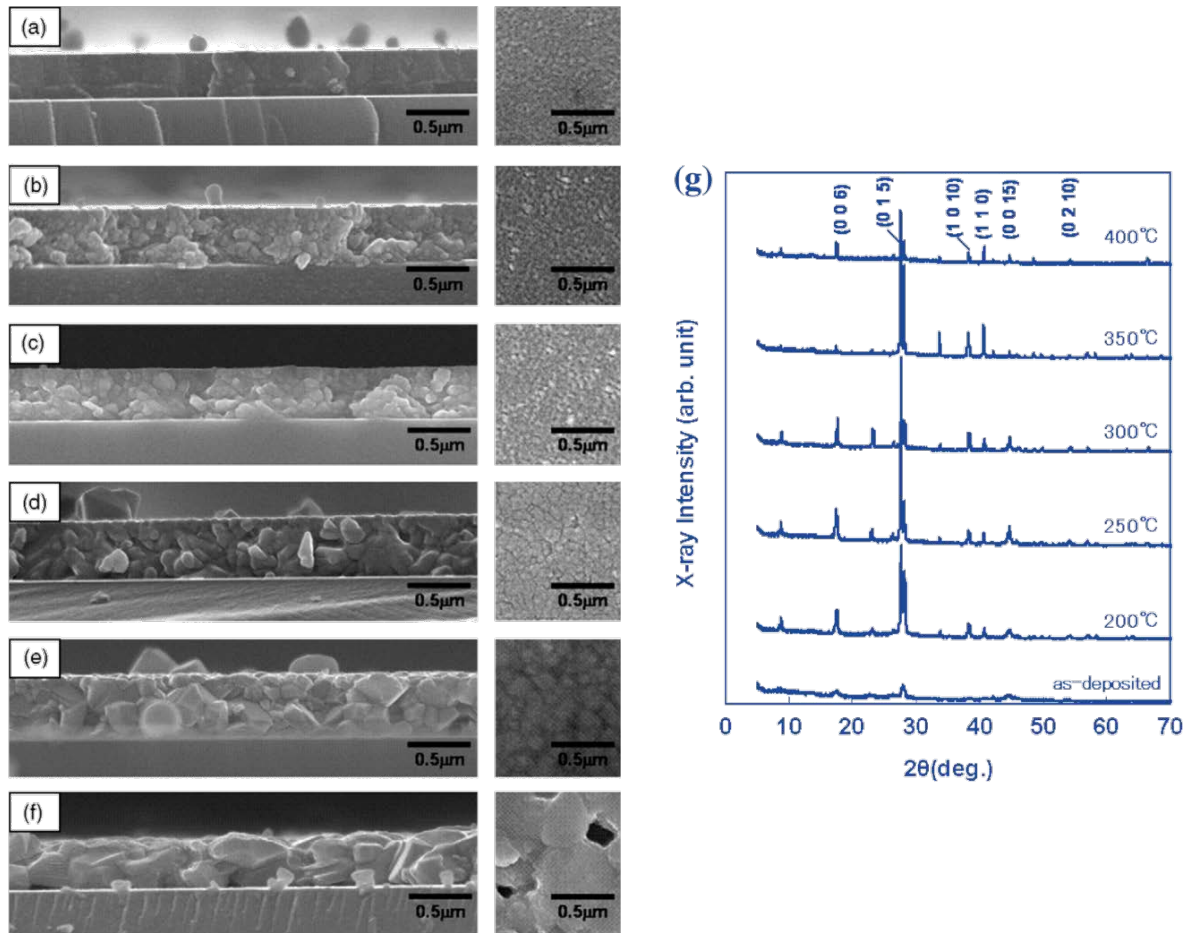
Figure 11. Cross-section and surface morphology of $Bi_{0.4}Sb_{1.6}Te_{3.0}$ thin films fabricated by flash evaporation. (a) as-deposited; annealed at (b) 473 K; (c) 523 K; (d) 573 K; (e) 623 K; (f) 673 K; (g) XRD patterns.[54]

Although there have been many literature articles reporting thin-film fabrication techniques, Bi_2Te_3-based thin films prepared by these techniques do not exhibit high thermoelectric performance. Also, few research projects have been conducted to investigate the relationship between annealing and thermoelectric properties of Bi_2Te_3-based thin films fabricated by flash evaporation. To deeply understand the relationship between annealing and thermoelectric performance, research work from the authors has been performed to manufacture $Bi_{0.4}Sb_{1.6}Te_{3.0}$ thin films through flash evaporation combined with post-annealing.[54] In their experimental work, spherical $Bi_{0.4}Sb_{1.6}Te_{3.0}$ powders serve as the evaporation source, and 80 A of current serves as the evaporation power. Glass serves as the substrate, which is maintained at 473 K.

The evaporation source is 30 mm far from the glass substrate. The evaporation pressure in the chamber is 1.4×10^{-3} Pa. The deposition rate and thickness of as-deposited $Bi_{0.4}Sb_{1.6}Te_{3.0}$ thin films are 0.1 μm/s and 0.5 μm. Finally, the as-deposited $Bi_{0.4}Sb_{1.6}Te_{3.0}$ thin films are annealed at 473 K, 523 K, 573 K, 623 K, and 673 K respectively. Figure 11 illustrates the relationship between annealing and the crystal structure of $Bi_{0.4}Sb_{1.6}Te_{3.0}$ thin films. Figure 11(a) indicates the amorphous morphology of the as-deposited $Bi_{0.4}Sb_{1.6}Te_{3.0}$ thin films. This can be explained by the rapid deposition and thus, the re-crystallization in $Bi_{0.4}Sb_{1.6}Te_{3.0}$ thin films is insufficient. As annealing temperature rises, the crystallization and crystallite size increase (shown in Fig. 11(b)-(f)). However, when the as-deposited $Bi_{0.4}Sb_{1.6}Te_{3.0}$ thin films are annealed at 673 K, some porosity appears on the surface because of the evaporation of atoms. Similarly, Figure 11(g) illustrates the same result that post-annealing contributes to the crystallization of $Bi_{0.4}Sb_{1.6}Te_{3.0}$ thin films. It should be noticed that post-annealing also helps to produce highly-oriented $Bi_{0.4}Sb_{1.6}Te_{3.0}$ thin films, which can be confirmed by the stronger peak at (0 1 5) plane of $Bi_{0.4}Sb_{1.6}Te_{3.0}$ thin films as annealing temperature rising.

However, the distance between evaporation source and substrate should be adapted to an appropriate distance in order to obtain Bi_2Te_3-based thin films with clean surface. When investigating the fabrication and thermoelectric properties of $Bi_{0.4}Sb_{1.6}Te_{3.0}$ thin films, research from the authors has suggested that a distance of 200 mm results in a cleaner surface of $Bi_{0.4}Sb_{1.6}Te_{3.0}$ thin films than a distance of 30 mm.[55] This can be attributed to the incomplete melting of $Bi_{0.4}Sb_{1.6}Te_{3.0}$ powers when the distance (30 mm) is too short.

Like the post-annealing, hydrogen sintering after flash evaporation process also contributes to enhancing the crystalline structure of Bi_2Te_3-based thin films. Takashiri et al. have reported the preparation of p-type $Bi_{0.4}Sb_{1.6}Te_{3.0}$ and n-type $Bi_{2.0}Te_{2.7}Se_{0.3}$ thin films through flash evaporation followed by hydrogen sintering.[56] In their experimental work, spherical $Bi_{0.4}Sb_{1.6}Te_{3.0}$ and $Bi_{2.0}Te_{2.7}Se_{0.3}$ powders serve as the evaporation source, which are evaporated by 80 A of current. Glass serves as the substrates, which are maintained at 473 K. The distance between evaporation source and glass substrate is 200 mm. Before flash evaporation, the chamber is vacuumed to 1.4×10^{-3} Pa. Finally, the as-deposited films are sintered in hydrogen and argon atmosphere at temperature ranging from 473 K to 623 K for 30 minutes. Figure 12

summarizes the effect of sintering on the crystalline structure of thin films. It can be noticed that as the sintering temperature rises, XRD intensity increases, which means the enhanced crystallinity and consequent higher electrical conductivity. Research work from the authors has also reported the fabrication of similar $Bi_{0.4}Sb_{1.6}Te_{3.0}$ thin films and similar results that hydrogen sintering contributes to increased crystallinity.[57]
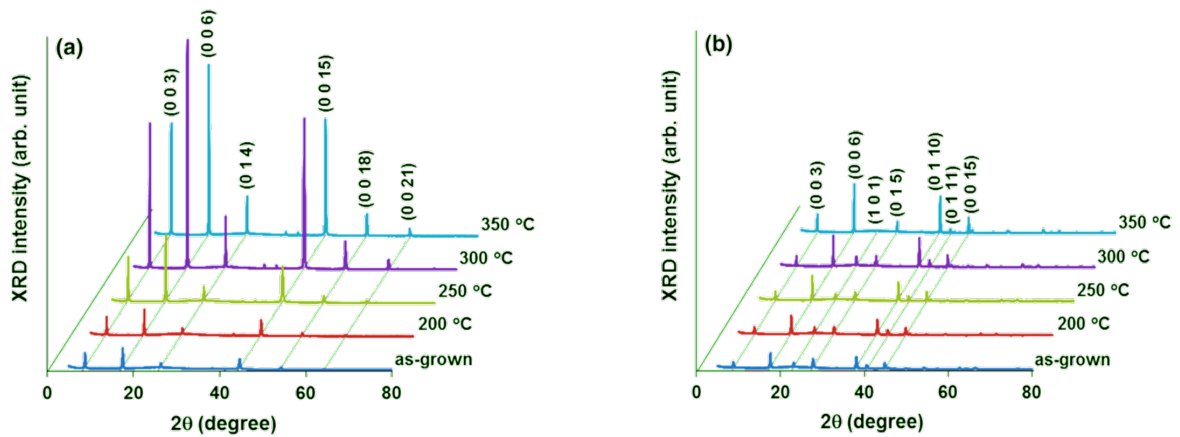
Figure 12. XRD Patterns of (a) $Bi_{0.4}Sb_{1.6}Te_{3.0}$ and (b) $Bi_{2.0}Te_{2.7}Se_{0.3}$ thin films fabricated by flash evaporation and sintered at different temperatures.[56]

To summarize, flash evaporation is a thin-film technique which is similar to thermal evaporation. The appropriate distance between evaporation source and substrate is 200 mm to produce Bi_2Te_3-based thin films with clean surface. In addition, annealing and sintering following flash evaporation help to enhance crystallinity of Bi_2Te_3-based thin films and consequently improve their thermoelectric performance. Bi_2Te_3-based alloys or powers are reported to be directly used to fabricate Bi_2Te_3-based thin films through flash evaporation in many literature articles. However, few literature articles report how to control the accurate stoichiometry of Bi_2Te_3-based thin films manufactured by flash evaporation. I suggest the use of individual elements during flash evaporation in order to obtain Bi_2Te_3-based thin films with accurate stoichiometry because of the different evaporation rate of elements. Thus, in the future research work, more efforts should be made to ensure the accurate stoichiometry of Bi_2Te_3-based thin films. In addition, elemental nanopowers are suggested to serve as the evaporation source in order to obtain high-performance nanocrystalline Bi_2Te_3-based thin films. Like thermal evaporation, evaporation rate should be controlled to optimize the morphology and

crystallization of Bi_2Te_3-based thin films because slow evaporation rate allows Bi_2Te_3-based thin films to have sufficient time to melt on tungsten and crystallize on substrates.

3.2.4. Electrochemical Deposition

Up to date, various synthesis techniques have been developed to prepare various Bi_2Te_3-based thermoelectric materials. Like solvothermal method, magnetron sputtering, thermal and flash evaporation methods, electrochemical deposition can also be implemented to manufacture Bi_2Te_3-based nanostructures and films. Furthermore, electrochemical deposition can work at room temperature and ambient pressure, which is more cost-efficiency and simple when compared with vacuum-based methods.[58] Thus, electrochemical deposition has been frequently applied to produce Bi_2Te_3-based thermoelectric materials with different morphology. Electrochemical deposition includes constant and pulsed ones. The difference between them is the applied potential. For constant electrochemical deposition, constant potential is applied. By contrast, a pulsed waveform (shown in Fig. 13) is applied during pulsed electrochemical deposition. The applied potentials alternate between E_{ON} cycle (potentiostatic mode) and I_{OFF} cycle (galvanostatic mode) during pulsed electrochemical deposition.[59] When E_{ON} is applied, amorphous material is deposited, while deposited material crystallizes when I_{OFF} is applied. This section aims to review Bi_2Te_3-based thermoelectric materials with different morphology (thick films and nanowires) which are prepared by electrochemical deposition. In the end, some recommendations are made.
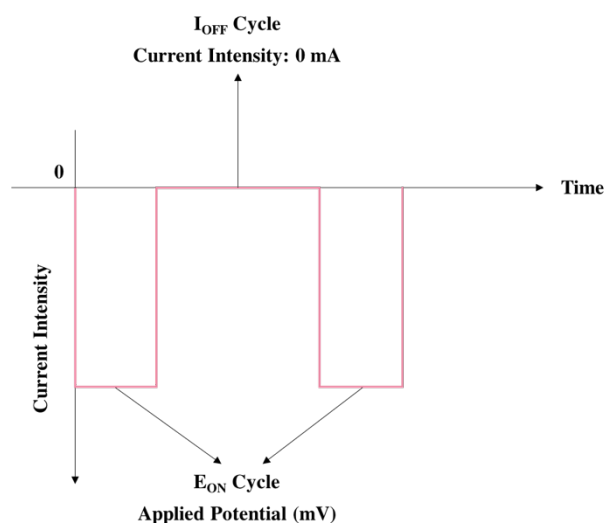
Figure 13. Waveform used in pulsed electrochemical deposition.[60]
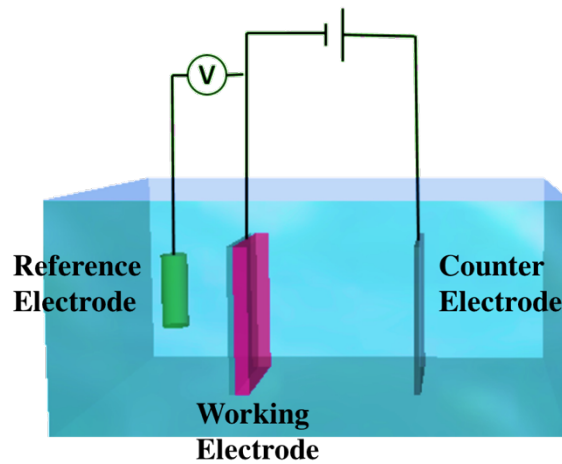
Figure 14. Conceptual model of electrochemical deposition system.[60]

Bi_2Te_3-based thick films have played an important role in fabricating high-efficiency thermoelectric power generators due to their high electrical properties. In addition, electrochemical deposition is advantageous to prepare Bi_2Te_3-based thick films in order to obtain compact films with high-quality surface morphology. Unfortunately, the Seebeck coefficient of Bi_2Te_3-based thick films prepared by this method is relatively low. This problem can be solved by the use of high-concentration non-aqueous electrolytes or Bi_2Te_3 soluble anode.[61,62] Another more environmental-friendly alternation is the use of low-concentration electrolyte. This can be explained by the lower deposition rate caused by low-concentration electrolyte. The lower deposition rate offers more time for Bi_2Te_3-based thick films to crystallize, which is attributed to better electrical properties. For instance, Trung et al. have reported the fabrication of high-performance Bi_2Te_3 and Sb_2Te_3 thick films through electrochemical deposition which uses the low-concentration solution as the electrolyte.[60] Their deposition process follows two stages: establishment of electrochemical deposition system and electrochemical deposition. During the first stage, Cr-Au films are deposited on Si substrate, which works as the working electrode, meanwhile the counter and reference electrodes are Pt mesh and Ag/AgCl with 3 M KCl solution respectively (shown in Fig. 14). During the second stage, low-concentration electrolyte is prepared firstly. For the deposition of Bi_2Te_3 thick films, Bi_2O_3 and TeO_2 are dissolved in HNO_3 respectively, followed by the addition of deionized water. These two formed solutions are mixed to form the low-concentration electrolyte. Similarly, for the fabrication of Sb_2Te_3 thick films, Sb_2Te_3 is dissolved in $C_4H_6O_4 \cdot 5H_2O$ and TeO_2 is dissolved in HNO_3 respectively, followed by the addition of deionized water. These two formed solutions

are mixed to form the low-concentration electrolyte. Finally, Bi_2Te_3 thick films are potentiostatically deposited by applying a potential of 20 mV meanwhile Sb_2Te_3 thick films are fabricated by pulsed electrochemical deposition which is powered by a waveform. Within this waveform, a potential of -144 mV is applied during the ON period for 0.1 s and a current of 0 mA is applied during the OFF period for 0.2 s.

Bi_2Te_3 nanowires produced by electrochemical deposition are desired for thermoelectric applications because these nanowires are high-density and show a small diameter, which helps to fabricate miniature thermoelectric devices. This type of nanowires is mainly produced by template-assisted electrochemical deposition, such as track-etched membranes and anodized aluminum oxide (AAO) templates.[63-66] AAO templates are more popular in template-assisted electrochemical deposition because they are simple and flexible to manufacture, but their high thermal conductivity and consequent thermal leakages limit their usages. Fortunately, polymer membranes, such as polycarbonate membranes, can be employed to serve as the templates due to their stable chemical, mechanical, thermal and electrical properties. For instance, research work from the authors has reported the fabrication of Bi_xTe_{1-x} nanowires on polycarbonate membranes through electrochemical deposition.[67] The fabrication of Bi_xTe_{1-x} nanowires includes two typical steps: template preparation and electrochemical deposition. In order to prepare templates, polycarbonate foils (PCF, 30 μm) are firstly irradiated by accelerated gold ions, resulting in ion tracks which are sensitized by UV exposure for 1 hour and then dissolved and enlarged by NaOH solution at a speed of 30 nm/min to produce pores with different diameter (30 nm, 60 nm and 120 nm). After chemical etching, platinum layer (160 nm) is deposited on one side of PCFs to act as the working electrode. During electrochemical deposition stage, electrolyte solution is firstly prepared. Te is oxidized to $HTeO_2^+$ in HNO_3 solution, and then $Bi(NO_3)_3$, distilled water and dimethyl sulfoxide (C_2H_6OS) are added into this formed solution to prepare electrolyte. Within the electrochemical deposition system, the previously prepared PCF works as working electrode, the counter and reference electrodes are platinum disc and saturated Ag/AgCl respectively. Before electrochemical deposition, 20-minute Ar flux is operated to remove the oxygen dissolved in electrolyte. Finally, Bi_xTe_{1-x} nanowires are potentiostatically electrodeposited at room temperature by using potentials of -
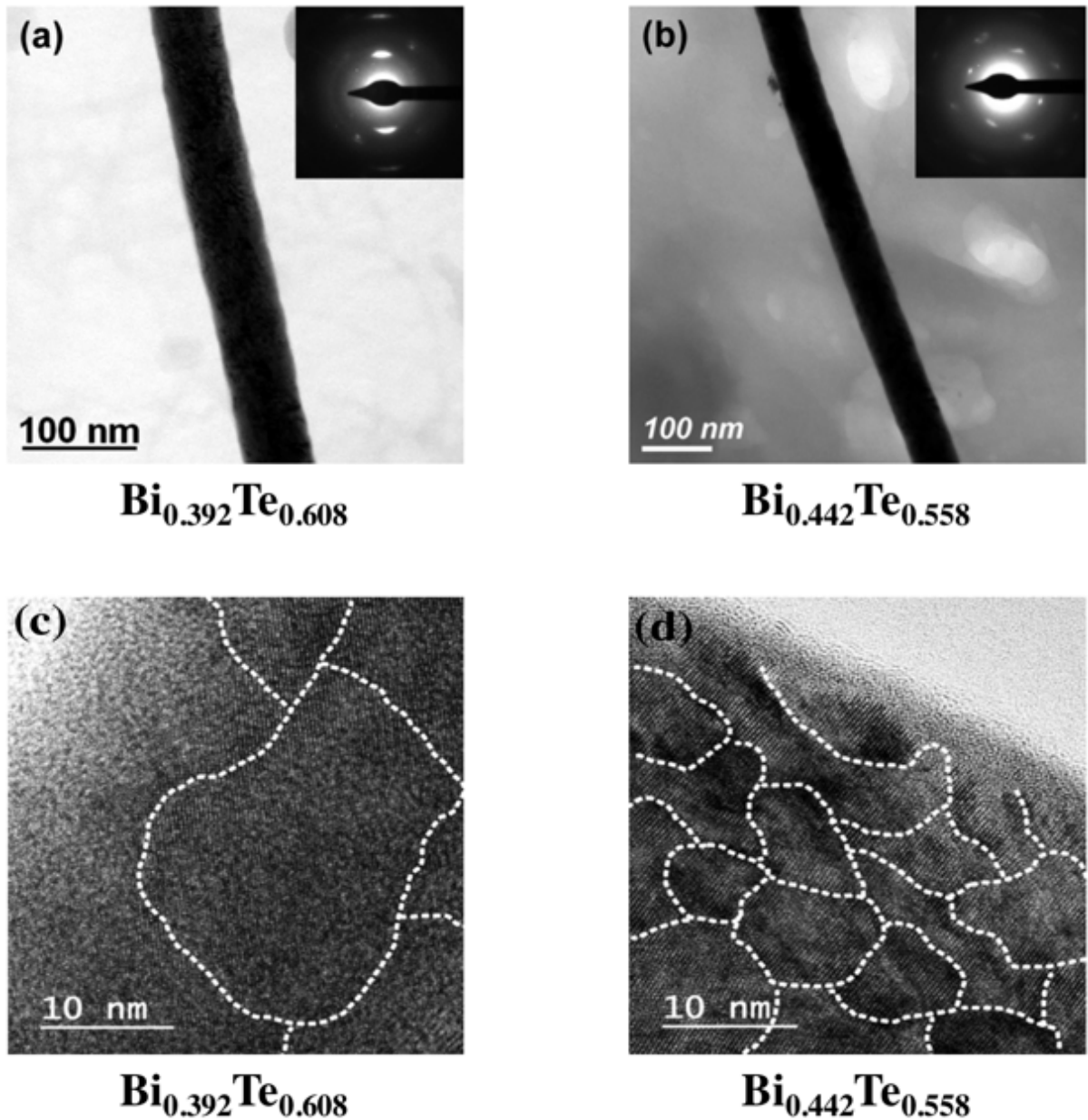
Figure 15. TEM images of Bi_xTe_{1-x} nanowires electrodeposited on PCF at (a) -75 mV and (b) -100 mV; HRTEM images of grain boundaries of Bi_xTe_{1-x} nanowires electrodeposited on PCF at (c) -75 mV and (d) -100 mV.[67]

75 mV and -100 mV respectively. The electrodeposited Bi_xTe_{1-x} nanowires are studied by transmission electron microscopy (TEM) as well as high-resolution transmission electron microscopy (HRTEM), and Figure 15 compares the morphology and grain boundaries of Bi_xTe_{1-x} nanowires. It can be noticed that the increasing cathodic potential results in Bi-rich Bi_xTe_{1-x} nanowires, and their grain sizes also increase with the increasing Te concentration. Since, nanowire diameter can be controlled by chemical etching and stoichiometry can be controlled by applied potentials, electrochemical deposition which employs track-etched

polymer membranes to be the templates is widely used to prepare Bi_2Te_3-based nanowires.

To summarize, electrochemical deposition is a simple and universal method to manufacture Bi_2Te_3-based thermoelectric materials with different morphology (thick films and nanowires). This method allows synthesis process to proceed at room temperature and pressure, which is cost-efficiency and simple. In addition, the use of low-concentration electrolytes contributes to obtain high-crystallinity Bi_2Te_3-based thermoelectric materials. However, few literature has studied the relationship between applied potentials and atomic composition. The future research work should be conducted to understand the dependence of stoichiometry on the potentials in order to control the atom ration within Bi_2Te_3-based thermoelectric materials.

3.3. High-Energy Ball Milling

Up to date, various synthesis techniques have been developed to manufacture Bi_2Te_3-based thermoelectric materials, such as solvothermal/hydrothermal method, wet chemical reactions and magnetron sputtering. Compared with these techniques, high-energy ball milling is more popular because of its commercialization and extensive industrial applications. Industrial manufacture often employs this method to manufacture fine nanoparticles or nanograins in large amount. In addition, this manufacture process is time-saving which is desired for industrial manufacture. High-energy ball milling can not only grind ingots into nanoparticles but also prepare nanoparticles directly from individual elements (mechanical alloying). Once nanoparticles are prepared, they are produced into nanocomposites by spark plasma sintering (SPS), hot-pressuring, cold-pressuring or extrusion methods.[68] Nanocomposites produced by cold-pressuring are often low-density and consequently exhibit poor mechanical performance. Thus, SPS and hot-pressuring are more attractive to produce nanocomposites, and these two methods are very similar. SPS is a pressure-assisted sintering process which is powered by pulsed direct current and is operated under high pressure, meanwhile hot-pressuring is also a pressure-assisted sintering powered by direct or alternating current. The combination of high-energy ball milling and sintering helps to produce high-efficiency bulk and nanostructured thermoelectric materials because of the production of small-size grains within materials, and thus this combination of techniques is more commonly used. This section intends to review and

evaluate bulk and nanostructured Bi_2Te_3-based thermoelectric materials prepared by high-energy ball milling.

During the synthesis process of high-efficiency bulk $Bi_{0.5}Sb_{1.5}Te_3$ prepared by Seo et al., a typical process is elucidated, which includes ball milling, hydrogen annealing and SPS.[32] At the stage of ball milling, a jar of attrition mills is vacuumed and filled by Ar in order to maintain a low oxygen concentration in the jar as oxygen will degrade thermoelectric properties of $Bi_{0.5}Sb_{1.5}Te_3$. Individual Bi, Sb and Te elemental chunks, which are weighted based on the stoichiometry of $Bi_{0.5}Sb_{1.5}Te_3$, are fed into the jar for the 24-hour ball milling (mechanical alloying) at a speed of 250 rpm. Hydrogen annealing of $Bi_{0.5}Sb_{1.5}Te_3$ powers is operated in 5% H_2-95% Ar gas flux for 1 hour at temperatures of 523 K, 673 K and 823 K. The annealed $Bi_{0.5}Sb_{1.5}Te_3$ powers are manually milled in a mortar to obtain fine powers which are then sintered by SPS system at 673 K under 40 MPa of high pressure for 10 minutes to produce bulk $Bi_{0.5}Sb_{1.5}Te_3$. The stoichiometry and phase of sintered bulk $Bi_{0.5}Sb_{1.5}Te_3$ samples are confirmed by energy dispersive spectroscopy (EDS) and XRD patterns (shown in Fig. 16) respectively. In the previous research work, bulk Bi_2Te_3, $BiSbTe_3$, n-type $Bi_2Te_{2.7}Se_{0.3}$, n-type $Bi_2Te_{3-y}Se_y$ (y=0.15-0.6) and p-type $Bi_{0.5}Sb_{1.5}Te_3$ have also been produced by mechanical alloying.[13,69-72]
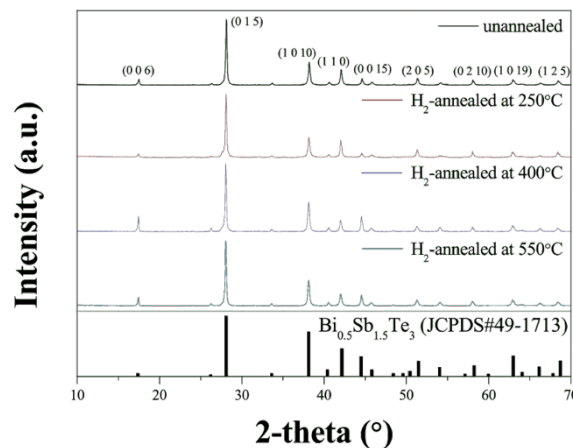
Figure 16. XRD patterns of $Bi_{0.5}Sb_{1.5}Te_3$ samples prepared by ball milling and hydrogen annealed at 523 K, 673 K and 823 K.[32]

Like ball milling combined with hot pressuring, planetary milling combined with hot pressuring is also often applied to manufacture Bi_2Te_3-based alloy solid solutions. For instance, Eum et al. have reported the successful preparation of n-type $Bi_2Te_{3-y}Se_y$ through this synthesis process.[33]

This process is very similar to ball milling combined with hot pressuring. High-purity individual Bi, Te and Se elements are weighted according the atomic ratio of $Bi_2Te_{3-y}Se_y$ (y=0-0.6), mixed with steel balls and then fed into a planetary mill which is filled with Ar gas. The planetary milling or mechanical alloying is operated at a speed of 300 rpm for 8 hours. Finally, the milled powers are hot-pressed into bulk $Bi_2Te_{3-y}Se_y$ (y=0-0.6) samples. The hot-pressed bulk $Bi_2Te_{3-y}Se_y$ (y=0-0.6) samples show a relative density of 96%. In addition, $Bi_2Te_{3-y}Se_y{:}I_m$ (y=0.15-0.6 and m=0.0025-0.01) and p-type $(Bi, Sb)_2Te_3$ have also been produced by this synthesis process.[73,74]

Previous research work has also reported the great improvement in thermoelectric performance of Bi_2Te_3-based nanostructures manufactured by high-energy ball milling.[75] For example, ball-milling combined with hot pressure can be applied to produce nanocrystalline (NC) $Bi_{05}Sb_{1.5}Te_3$ with large ZT values.[76] Crystalline $Bi_{05}Sb_{1.5}Te_3$ alloy ingots are ball-milled into $Bi_{05}Sb_{1.5}Te_3$ nanopowers in a jar which is previously filled by Ar gas in order to remove oxygen and ensure the high electrical transport properties. Once $Bi_{05}Sb_{1.5}Te_3$ nanopowers are prepared, they are compacted into bulk NC $Bi_{05}Sb_{1.5}Te_3$ by hot-pressuring. The produced bulk NC $Bi_{05}Sb_{1.5}Te_3$ exhibits a high ZT of 1.4 at 373 K. This can be explained by both the high crystallinity (which contributes to high electrical transport properties) and the increased boundary density (which contributes to the increased phonon scattering and consequent thermal conductivity reduction).

To summarize, high-energy ball milling is commonly used to manufacture bulk and nanostructured Bi_2Te_3-based thermoelectric materials because it is industrially commercialized, time-saving and can be used to produce large quantity of Bi_2Te_3-based alloy solutions. In addition, the precursors of ball milling can be not only Bi_2Te_3-based alloys but also individual elements. Furthermore, the Bi_2Te_3-based thermoelectric materials prepared by high-energy ball milling tend to exhibit high-thermoelectric performance, which mainly benefits from thermal conductivity reduction caused by small-size grains within these prepared materials. The only weakness of ball milling is that this technique cannot fabricate Bi_2Te_3-based films. For the application of high-energy ball milling, three suggestions are made: (1) individual elemental chunks are suggested to serve as the starting materials because this can contribute to controlling

accurate stoichiometry of Bi_2Te_3-based thermoelectric materials; (2) starting materials are suggested to be crystalline because high-crystallinity thermoelectric materials can exhibit high electrical transport properties; and (3) atmosphere during ball milling is suggested to be low-oxygen as oxygen content will degrade thermoelectric properties of Bi_2Te_3-based materials.

4. Thermoelectric Performance Improvement of Bi₂Te₃-Based Materials

As mentioned previously, thermoelectric power generation can be a promising solution to the ever-increasing energy demand and storages, and various synthesis processes have been applied to prepare Bi_2Te_3 and its alloys. Therefore, fabricating high-efficiency thermoelectric devices is important in order to efficiently convert waste heat to electricity energy. High-thermoelectric performance of Bi_2Te_3-based alloys is required to fabricate such thermoelectric devices. In other words, improving thermoelectric performance of Bi_2Te_3-based alloys is important and urgent. Thermoelectric performance can be described by the dimensionless thermoelectric figure of merit, ZT, which is calculated by Eq. (1). In theory, thermoelectric efficiency of Bi_2Te_3-based alloys can be as high as like. However, ZT values of state of art p-type and n-type Bi_2Te_3-based thermoelectric materials are approximately 0.8 and 0.5 respectively, and a ZT more than unity is required for practical applications. Fortunately, ZT can be improved by increased electrical conductivity, increased Seebeck coefficient and/or thermal conductivity reduction, and Figure 17 summarizes some ZT improvement of Bi_2Te_3-based materials. It can be noticed that ZT values of p-type Bi_2Te_3-based thermoelectric materials can be improved from around 0.8 to 1.5, meanwhile those of n-type Bi_2Te_3-based thermoelectric materials can be improved from around 0.5 to 1.0. However, it remains challenging to improve $ZT>2$. Indeed, the big challenge of improving ZT to 2.0 is due to the interdependence of thermoelectric parameters, such as the conflict between electrical conductivity and Seebeck coefficient and the conflict between electrical and lattice thermal conductivities.[77] These conflicts are due to the conflicting relationships among electrical conductivity, Seebeck coefficient, lattice thermal conductivity and carrier concentration.[78] Electrical conductivity and Seebeck coefficient are defined by Eqs. (6) and (7),

$$\sigma = ne\mu, \tag{6}$$

$$S = \frac{8\pi^2 k_B^2}{3eh^2} m_1^* T \left(\frac{\pi}{3n}\right)^{2/3}, \tag{7}$$

where $\sigma, n, e, \mu, S, k_B, h, \ m_1^*$ and T are electrical conductivity, carrier concentration, elementary
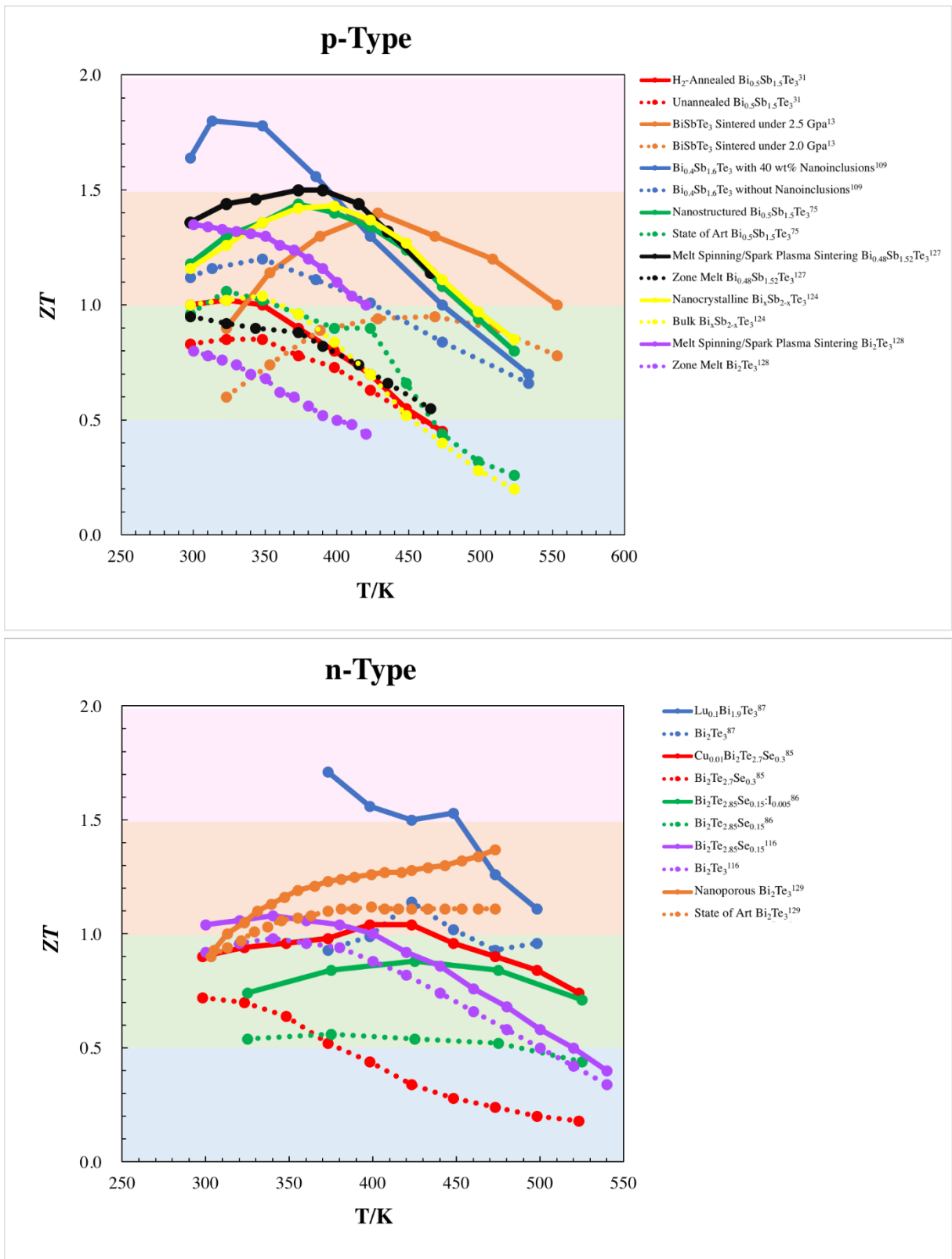
Figure 17. Comparison of after-improved (full lines) and before improved (dotted lines) *ZT* of p-type and n-type Bi_2Te_3-based thermoelectric materials.

charge, carrier mobility, Seebeck coefficient, Boltzmann constant, Planck constant, transport mass in the conduction direction and absolute temperature respectively.[8,79] Therefore, carrier

concentration has positive effect on electrical conductivity but negative effect on Seebeck coefficient. In addition, carrier mobility is calculated by Eq. (8),

$$\mu = e\tau/m_1^*,\qquad\qquad(8)$$

where μ, τ and m_1^* are carrier mobility, carrier relaxation time and transport mass in the conduction direction respectively. Thus, transport mass has negative effect on carrier mobility and consequent negative effect on electrical conductivity, but a high transport mass is necessary for high Seebeck coefficient. Furthermore, increased scattering has positive effect on lattice thermal conductivity reduction, but it decreases electrical conductivity simultaneously. Therefore, it is challenging to improve $ZT > 2$, and this section aims to review and summarize different current strategies to enhance ZT of Bi_2Te_3-based thermoelectric materials.

4.1. Electrical Conductivity Improvement

As described in Eq. (6), high carrier concentration and mobility are desired to enhance electrical conductivity, and an electrical conductivity on the order of 10^5 S/m is necessary for high-performance thermoelectric materials. Thus, this sub-section intends to review and evaluate how to enhance carrier concentration and mobility in Bi_2T_3-based thermoelectric materials.

4.1.1. Maximizing Carrier Concentration

High-performance Bi_2T_3-based thermoelectric materials usually require a carrier concentration ranging from 10^{19} to 10^{21} cm^{-3},[80] and increasing carrier concentration is a traditional strategy to improve ZT of Bi_2T_3-based thermoelectric materials. In addition, doping and point defects (including vacancy and antisite defects) are the main methods to manipulate the carrier concentration.

Doping: Doping has been extensively investigated by previous research work in order to increase carrier concentration and resultant high ZT.[81-84] For example, Han et al. have prepared Bi_2Te_3 doped with Cu and the prepared $Cu_{0.07}Bi_2Te_3$ has a ZT of 1.15 at 300 K;[85] Liu et al. have reported n-type $Bi_2Te_{2.7}Se_{0.3}$ doped with Cu and the prepared $Cu_{0.01}Bi_2Te_{2.7}Se_{0.3}$ has a maximum ZT of 1.10 at 423 K;[86] and Lee et al. have reported the improved ZT of 0.90 at 423 K for n-type $Bi_2Te_{2.85}Se_{0.15}$:$I_{0.005}$.[87] Typically, Yang et al. have reported an improvement of

carrier (electron) concentration in n-type nanostructured lutetium-doped $Lu_xBi_{2-x}Te_3$, resulting in enhancement of electrical conductivity, power factor and ZT.[88] Figure 18(a) illustrates that $Lu_{0.1}Bi_{1.9}Te_3$ and $Lu_{0.25}Bi_{1.75}Te_3$ exhibit lower electrical resistivity, compared with Bi_2Te_3. This results from the increased carrier (electron) concentration by doping. But, $Lu_{0.4}Bi_{1.6}Te_3$ has not shown any improvement of electrical conductivity, compared with Bi_2Te_3, which can be explained by the limited doping amount and decreased carrier mobility caused by alloying scattering. Indeed, doping can result in alloying scattering which can increase phonon and electron scattering. The increased phonon scattering as well as the nanostructuring in lutetium-doped $Lu_xBi_{2-x}Te_3$ contribute to a low thermal conductivity. However, as described in Eq. (7), the increased carrier concentration induced by doping has negative effect on Seebeck coefficient and results in slightly decreasing Seebeck coefficient. Fortunately, the decreased electrical resistivity can overcompensate the slightly decreased Seebeck coefficient, and thus the power factor and ZT has been improved (illustrated in Fig. 18(b)-(c)). Eventually, n-type nanostructured lutetium-doped $Lu_{0.1}Bi_{1.9}Te_3$ can obtain an optimized ZT of 1.7 at 373 K, which is an important thermoelectric performance enhancement when comparing with undoped Bi_2Te_3.
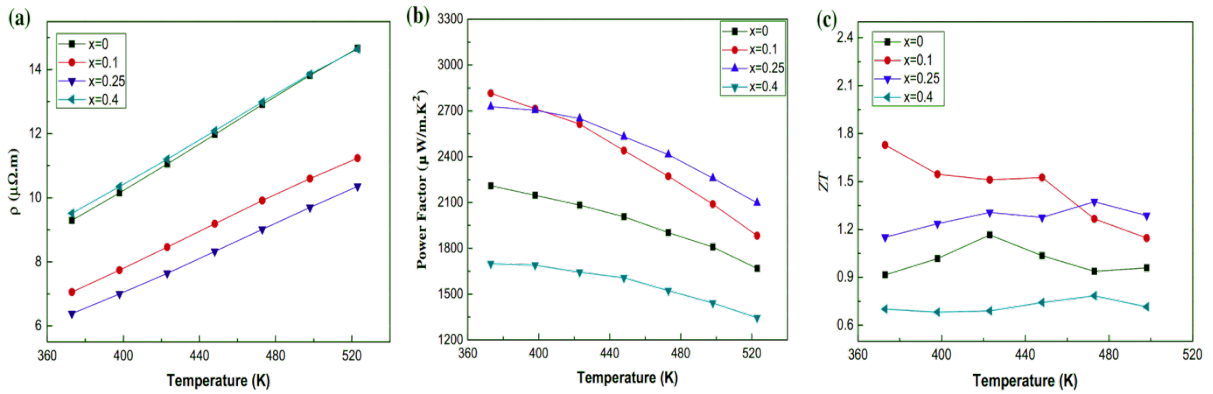
Figure 18. (a) Electrical conductivity, (b) power factor and (c) ZT of nanostructured lutetium-doped $Lu_xBi_{2-x}Te_3$ with respect to temperature.[88]

Antisite defects: Point defects, especially antisite defects, have been extensively applied to enhance the carrier concentration and resultant thermoelectric efficiency.[89-91] For example, Seo et al. have reported an improvement of carrier (hole) concentration in ball-milled and hydrogen annealed p-type $Bi_{0.5}Sb_{1.5}Te_{3.0}$, resulting in electrical conductivity increment of 30%, power

factor increment of 27.0% and *ZT* increment of 18.2%.[32] In their experimental work, $Bi_{0.5}Sb_{1.5}Te_{3.0}$ is prepared by the traditional combination technique of high-energy ball milling and sintering. However, dissolving oxygen into $Bi_{0.5}Sb_{1.5}Te_{3.0}$ cannot be avoided during the high-energy ball milling, and consequently electrical transport properties are degraded by the dissolved oxygen content. As a result, hydrogen annealing can be performed at temperatures of 523 K, 673 K and 823 K to remove the dissolved oxygen in order to increase antisite defects and thus obtain a high *ZT* of $Bi_{0.5}Sb_{1.5}Te_{3.0}$. Figure 19(a) shows the decrease of oxygen content with respect to H_2-annealing temperature, meanwhile Figure 19(b) shows the increase of carrier concentration with respect to H_2-annealing temperature which contributes to enhancing electrical conductivity (illustrated in Fig. 20(a)). The improved carrier concentration originates from both thermal annealing and decreased oxygen content. As mentioned in Section 2.2, the increasing high temperature caused by thermal annealing contributes to the increased antisite defects Bi'_{Te} and/or Sb'_{Te} concentration which leads to the increment of carrier (hole) concentration. In addition, oxygen dissolved in $Bi_{0.5}Sb_{1.5}Te_{3.0}$ occupies Te sites and serves as a donor, which increases the minority carrier (electron) concentration in $Bi_{0.5}Sb_{1.5}Te_{3.0}$ and thus reduces electrical conductivity in p-type $Bi_{0.5}Sb_{1.5}Te_{3.0}$. Therefore, oxygen content reduction induced by H_2-annealing is also attributed to the increased carrier concentration in $Bi_{0.5}Sb_{1.5}Te_{3.0}$. However, as mentioned previously, there are many conflicts between thermoelectric parameters. For example, according to Eq. (7), the increased transport mass but simultaneously increased carrier concentration result in a slight decrease in Seebeck coefficient. Similarly, although thermal annealing helps to increase antisite defects concentration, it also helps to increase the grain sizes, which results from coarsening induced by thermal energy. As a result, there is a decrease in the boundary density and grain boundary scattering for phonons is suppressed, which results in a small increment of lattice thermal conductivity. Eventually, a large increment of electrical conductivity (30%) together with slightly decreased Seebeck coefficient as well as slightly increased lattice thermal conductivity is achieved by increasing antisite defects induced by hydrogen annealing at 673 K, and 27.0% of power factor enhancement (shown in Fig. 20(b)) as well as 18.2% of *ZT* enhancement (shown in Fig. 20(c)) are achieved. In addition to H_2-annealing, an appropriate Sb concentration in $Bi_xSb_{2-x}Te_3$ can also be used to optimize antisite defect concentration and consequent carrier concentration.[92-94]
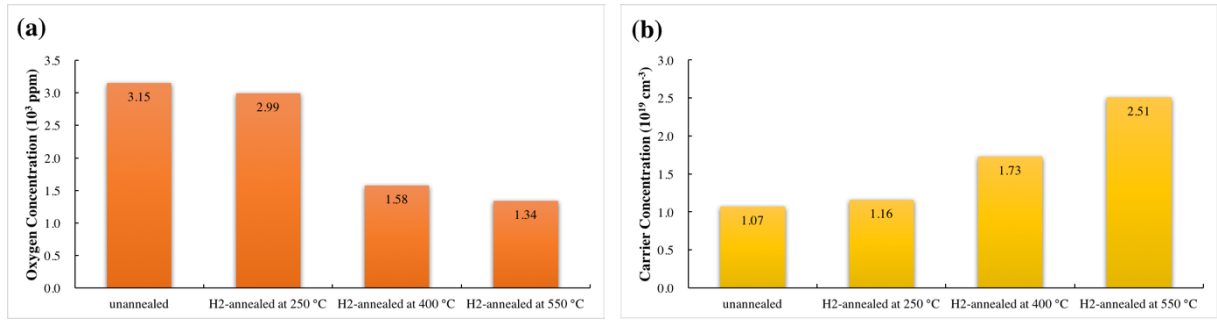
Figure 19. (a) Oxygen concentration and (b) carrier concentration in ball-milled and H_2-annealed $Bi_{0.5}Sb_{1.5}Te_{3.0}$ with respect to H_2-annealling temperature.[32]
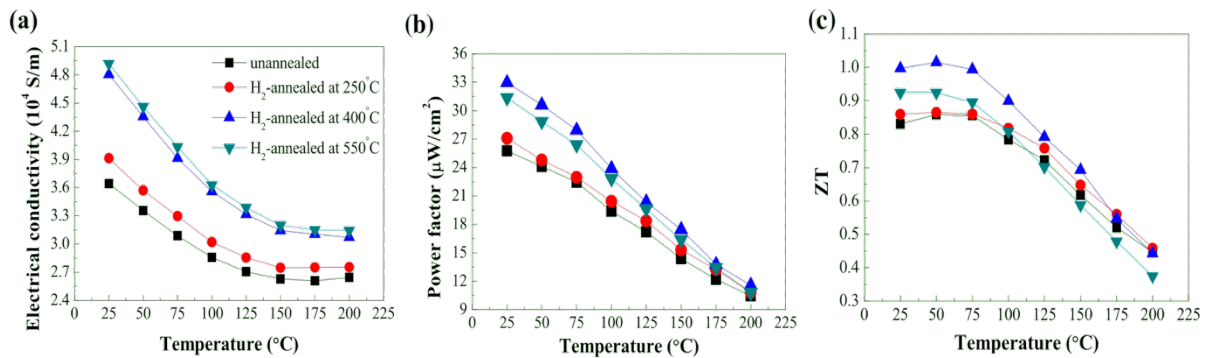
Figure 20. (a) Electrical conductivity, (b) power factor and (c) *ZT* of ball-milled and H_2-annealed $Bi_{0.5}Sb_{1.5}Te_{3.0}$ with respect to temperature.[32]

To summarize, doping and antisite defects are the most important strategies to improve carrier concentration in Bi_2Te_3-based thermoelectric materials and consequently elevate their thermoelectric efficiency, and hydrogen annealing as well as addition of Sb can be employed to increase antisite defects. However, ones still do not have a clear insight into the category of dopants that can maximally increase carrier concentration, although currently Cu is the most popular dopants. In addition, each single dopant should have a dissolution limit in Bi_2Te_3-based thermoelectric materials, and this limit should be clearly identified in order to avoid excessive doping because excessive doping cannot further increase carrier concentration but suppress carrier mobility.

4.1.2. Maximizing Carrier Mobility

A high level of carrier mobility is necessary for high-performance Bi_2T_3-based thermoelectric materials, although they often already possess a high level of carrier concentration. Electronic

structure and various scattering, such as phonon scattering, ionized impurity scattering and grain boundary scattering, have important impact on the carrier mobility. In addition, as described in Eq. (8), a high level of carrier mobility requires a high carrier relaxation time which can be realized by suppressing various existing scattering within Bi_2T_3-based thermoelectric materials. Thus, minimizing scattering is the main method to improve carrier mobility.

Phonon scattering: Phonon scattering is the main scattering in Bi_2T_3-based thermoelectric materials, and as mentioned previously, there are considerable conflicts between carrier transport and phonon transport properties. Deformation potential can be used to describe the strength of these conflicts.[95,96] Deformation potential scattering from phonons means that phonon wave can cause a strain in the crystal lattice when moving through the crystal lattice. The strain induced by phonon wave movement contributes to disturbing the energy bands and resultant scattering of carriers.[97] The resultant carrier scattering has negative influence on carrier mobility, and thus a low deformation potential is required to enhance carrier mobility, which is suggested by the relationship between carrier mobility and deformation potential, $\mu \propto \frac{C_1}{m_1^* (m_b^*)^{3/2} \, \Xi^2 \, T^{3/2}}$, where μ, C_1, m_1^*, m_b^*, Ξ, and T are carrier mobility, average longitudinal elastic modulus, transport mass in the conduction direction, density of states (DOS) effective mass, deformation potential coefficient and absolute temperature.[8] In other words, reducing the strain caused by phonon wave movement in the crystal lattice can contribute to carrier mobility improvement.

Ionized impurity scattering: Since doping is a universal strategy to improve carrier concentration and resultant thermoelectric performance of Bi_2Te_3-based solid solutions, various ionized impurities will reside in the crystal lattice, which contributes to increasing the scattering centres for carriers and consequently decreasing carrier mobility. Fortunately, in theory, modulation doping can serve as a good strategy to not only improve carrier concentration but also remain a high carrier mobility in Bi_2Te_3-based solid solutions. Modulation doping means that carriers can be separated from their origin atoms (dopants) when dopants are introduced into the crystal lattice.[8] In detail, heavily doped minor phases are introduced into the undoped matrix of Bi_2Te_3-based materials, followed by appropriate band alignment which results in moving carriers from the heavily doped phases to the undoped matrix. However, up to date,

there are not many literatures reporting the application of modulation doping in improving the thermoelectric performance of Bi_2Te_3-based materials, in addition to some applications in other thermoelectric materials, such as nanocomposites $(Si_{80}Ge_{20})_{70}(Si_{100}B_5)_{30}$.[98,99]

Grain boundary scattering: Grain boundary scattering for carriers is another important scattering mechanism and it is relatively easy to be suppressed in order to increase carrier mobility and consequent thermoelectric performance of Bi_2Te_3-based materials. In addition, since nanostructuring has been extensively implemented to reduce thermal conductivity of Bi_2Te_3-based thermoelectric materials, carrier scattering from grain boundaries cannot be ignored, especially when the grain sizes are approximately equal to or bigger than the mean free path of carriers. Therefore, it is important and necessary to supress this carrier scattering by aligning the random grain boundaries (crystal lattice) which can help carriers to transport from the hot to cold ends. In other words, highly-oriented c-axis crystal growth of Bi_2Te_3-based thermoelectric materials is required as Bi_2Te_3-based alloys exhibit anisotropy in structure characteristics, as mentioned in Chapter 2. Although the grain boundaries are reconstructed to be highly c-axis oriented, the density of grain boundaries is not reduced and thus grain boundary scattering for phonons remain at a high level. In particular, in order to enhance carrier mobility, aligning grain boundaries has more noticeable impact on polycrystalline Bi_2Te_3-based thermoelectric materials because polycrystalline Bi_2Te_3-based alloys usually possess more random grain boundaries when compared with single-crystal ones. Indeed, texture engineering is an important method to reconstruct grain boundaries in Bi_2Te_3-based thermoelectric materials, such as spark plasma sintering (SPS), hot pressing (HP), hot deformation (HD) and shear extrusion.

Many literatures have reported the use of high crystal orientation in improving thermoelectric properties of Bi_2Te_3-based materials.[100-102] For example, Yamauchi and Takashiri have reported the highly-oriented Bi_2Te_3 thin films which exhibit high carrier mobility.[19] These Bi_2Te_3 thin films are firstly deposited by radio frequency (RF) magnetron sputtering and then are treated by electron beam (EB) irradiation and thermal annealing. As mentioned previously, Lotgering
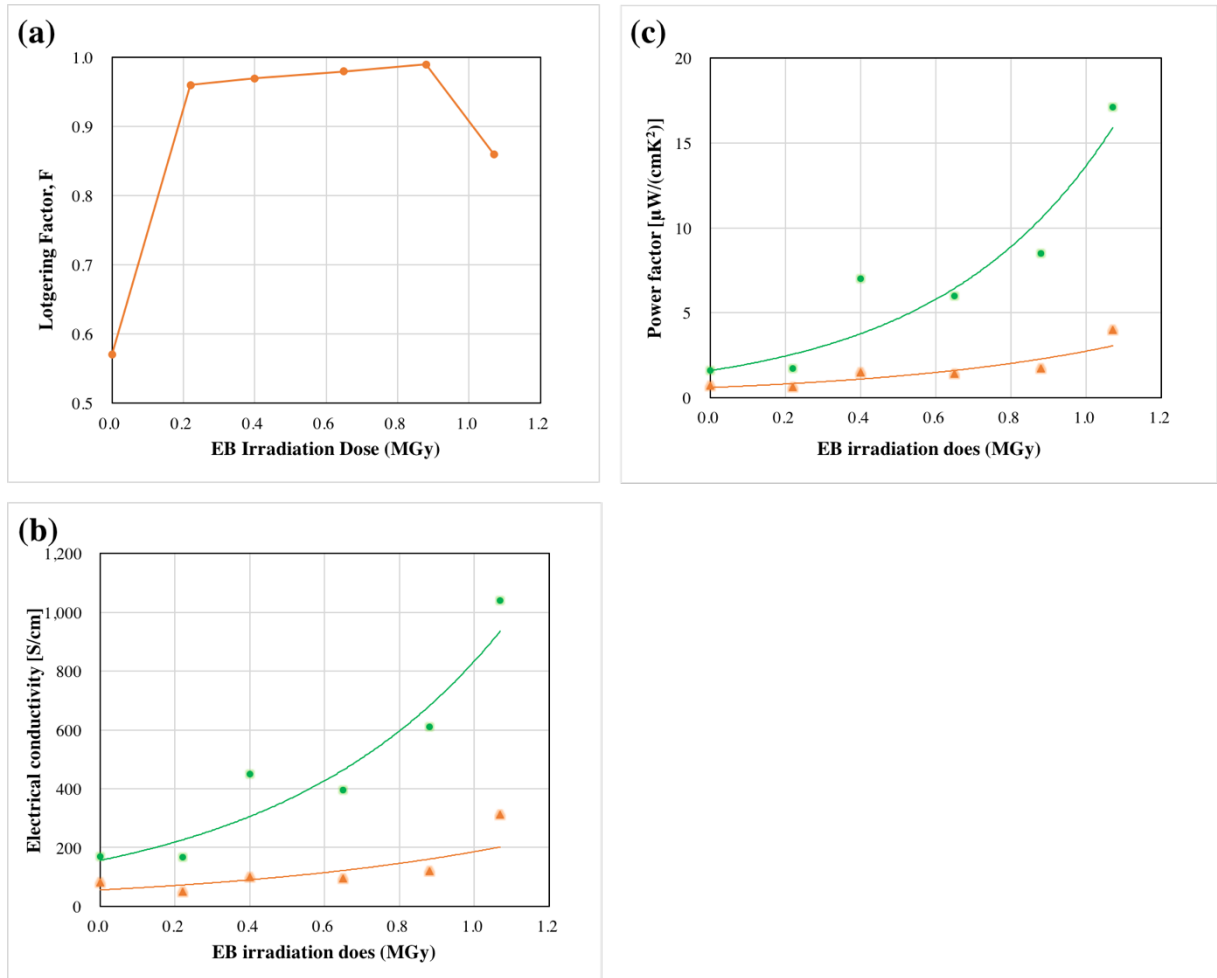
Figure 21. (a) Plot of Lotgering Factor vs. EB irradiation dose, (b) electrical conductivity and (c) power factor with respect to EB irradiation dose (green and yellow lines represent in-plane and cross-plane properties respectively).[19]

factor, F, can be used to describe the degree of orientation along c-axis. Figure 21(a) indicates that EB irradiation helps to prepare highly-oriented Bi_2Te_3 thin films and a highest Lotgering factor of 0.99 can be obtained by 0.87 MGy of EB irradiation. In addition, Figure 21(b) and (c) illustrate the increase in electrical conductivity and resultant power factor with increasing EB irradiation dose (increasingly high crystal orientation). Since electrical conductivity is decided by carrier concentration and mobility, the improvement in electrical conductivity of highly-oriented Bi_2Te_3 thin films is mainly due to the improved carrier mobility. Therefore, high crystal orientation contributes to improving carrier mobility and consequent electrical conductivity. Interestingly, the highest electrical conductivity and power factor are achieved at 1.07 MGy of EB irradiation dose, instead of 0.86 MGy at which Bi_2Te_3 thin films have the highest crystal orientation. This can be explained by the fact that the increased EB irradiation

leads to melting and interconnecting of Bi_2Te_3 grains especially when EB irradiation dose is more than 0.87 MGy. The increased interconnection of Bi_2Te_3 grains has more important influence on electrical conductivity than the crystal orientation. Eventually, highly-oriented Bi_2Te_3 thin films can achieve an in-plane power factor as high as 17.1 $\mu W/(cm·K^2)$. However, not only electrical but also thermal conductivities are anisotropic.[101] Indeed, thermal conductivity also increases with respect to degree of crystal orientation, but degree of crystal orientation almost has no influence on Seebeck coefficient because Seebeck coefficient is determined by band structure rather than degree of crystal orientation.[50] Therefore, only a small enhancement can be made in *ZT* values as both electrical and thermal conductivities increase with increasing degree of crystal orientation.

To summarize, optimizing carrier mobility can be realized by maximally suppressing various existing scattering mechanism (especially phonon scattering, ionized impurity scattering and grain boundary scattering) in Bi2Te3-based thermoelectric materials. Suppressing carrier scattering from grain boundary can be realized by reconstructing random grain boundaries (crystal lattice), such as EB irradiation. In order to suppress phonon scattering, the strain caused by phonon wave movement in the crystal lattice should be minimized. Similarly, in order to suppress ionized impurity scattering, modulation doping can be applied at the stage of maximizing carrier concentration. However, the latter two newly developed strategies have not been applied to optimize carrier mobility in Bi2Te3-based thermoelectric materials. Therefore, the future research work should attach emphasis on these newly developed strategies in order to further pave roads to improve thermoelectric performance of Bi2Te3-based materials.

4.2. Seebeck Coefficient Improvement

Although a high electrical conductivity is achieved by high carrier concentration and/or mobility in order to prepare high-performance Bi_2Te_3-based thermoelectric materials, Seebeck coefficient improvement cannot be ignored because Seebeck coefficient has more influence on *ZT* values, which is described by Eq. (1). In addition, when carrier concentration is fixed in Bi_2Te_3-based thermoelectric materials, Seebeck coefficient is determined by total density of states (DOS) effective mass which is calculated by Eq. (9),

$$m_d^* = N_V^{2/3} m_b^*, \tag{9}$$

where m_d^*, N_V and m_b^* represent total DOS effective mass, band degeneracy and DOS single-valley effective mass respectively.[8] In particular, doping or alloying of Bi_2Te_3-based solid solutions contributes to band flattening, which leads to the increment of DOS single-valley effective mass and consequent increase in DOS effective mass as well as Seebeck coefficient.

As described in Eq. (9), apart from the improvement of DOS single-valley effective mass, enhancement of band degeneracy can be employed to increase total DOS effective mass and consequently optimize Seebeck coefficient. In fact, Bi_2Te_3 with a high value of *ZT* tends to possess a high value of band degeneracy.[8] Furthermore, band convergence is an important strategy to increase band degeneracy, and band convergence can occur if two or more bands exhibit the same or similar energy, which includes orbital and valley degeneracy. In other words, there are two important strategies to realize band convergence: convergence from different bands through alloying with particular atoms or elevating temperature (orbital degeneracy) and tuning symmetry of crystals (valley degeneracy), such as valley degeneracy in $Bi_xSb_{2-x}Se_3$.[103-106]

Energy-filtering effect can also be used to optimize Seebeck coefficient. Energy-filtering effect refers to the fact that the bands of nanostructures introduced into Bi_2Te_3-based materials can align with the bands of the Bi_2Te_3-based materials in a manner than can prevent low-energy carriers from transporting (shown in Fig. 22(a)).[107] As a result, the filtering out of low-energy carriers by the small energy barriers (introduced nanostructures) contributes to a large differential conductivity and resultant optimized Seebeck coefficient.[108,109] For instance, Guo et al. have reported the implementation of energy-filtering effect to obtain high Seebeck coefficient and consequent high *ZT* values of $BiSbTe_3$.[13] In their experimental work, $BiSbTe_3$ is prepared by high pressure sintering technique which introduce energy barriers into $BiSbTe_3$. As shown in Fig. 22(b), $BiSbTe_3$ sintered under 2.5 GPa possesses a higher Seebeck coefficient than that under 2 GPa. This results from the higher energy barrier concentration in $BiSbTe_3$ sintered under 2.5 GPa, and thus low-energy carriers are filtered out more efficiently. Eventually, $BiSbTe_3$ sintered under 2.5 GPa exhibits a better thermoelectric performance (a higher *ZT*) (shown in Fig. 22(c)), although the considerable improvement in Seebeck coefficient

is accompanied with slight variation in thermal conductivity. A similar but more successful improvement in Seebeck coefficient and resultant ZT ($ZT = 1.8$ at 323 K) has been reported for p-type $Bi_{0.4}Sb_{1.6}Te_3$ nanocomposites with nanoinclusions.[109]
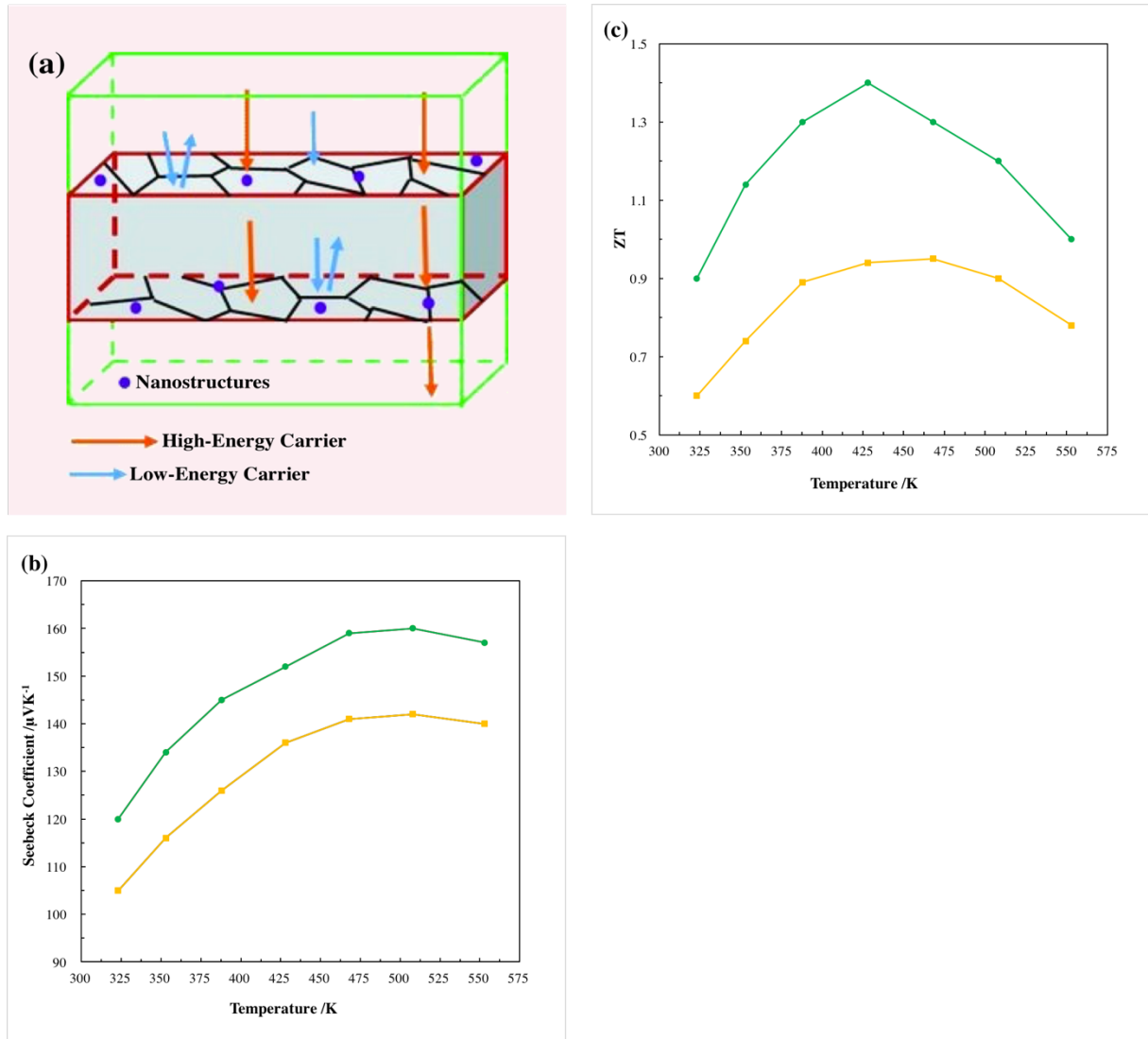
Figure 22. (a) Schematic illustration of energy filtering effect, (b) Seebeck coefficient and (c) ZT of $BiSbTe_3$ prepared by sintering under 2 GPa (yellow lines) and 2.5 GPa (green lines).[13,110]

Another crucial strategy to optimize Seebeck coefficient is the use of ionized impurity scattering for carriers. As mentioned previously, ionized impurities in Bi_2Te_3-based alloys can act as scattering centers for carriers. In particular, low-energy carriers can be effectively scattered by these ionized impurity centers and then filtered out, which contributes to improvement of Seebeck coefficient.[111] However, carrier scattering from ionized impurities also leads to suppressed carrier mobility and resultant decreased electrical conductivity.

Fortunately, when evaluating the thermoelectric performance, improvement of Seebeck coefficient induced by ionized impurity scattering can compensate or even overcompensate for the negative effect on electrical conductivity. Therefore, controlling appropriate ionized impurity concentration in Bi_2Te_3-based thermoelectric materials is very crucial to benefit the most from ionized impurity scattering.[112]

To summarize, the most practical strategy to optimize Seebeck coefficient is high pressure sintering techniques which can result in high energy barrier concentration in Bi_2Te_3-based thermoelectric materials. The resultant high energy barrier concentration contributes to increasing Seebeck coefficient through energy-filtering effects. In addition, doping and/or alloying can enhance DOS single-valley effective mass, and band convergence results in band degeneracy, both of which lead to maximize Seebeck coefficient. However, these two strategies currently have not been applied to practical cases. Furthermore, although ionized impurities have negative effect on carrier mobility, they contribute to increasing Seebeck coefficient. Therefore, in order to maximally improve *ZT* of Bi_2Te_3-based solid solutions, it is required to identify the appropriate concentration of ionized impurities in Bi_2Te_3-based alloys and thus benefit the most from ionized impurity scattering.

4.3. Thermal Conductivity Reduction

As described in Eq. (1), in addition to electrical conductivity and Seebeck coefficient, thermal conductivity is also an important thermoelectric parameter affecting the *ZT* values of Bi_2Te_3 and its alloys. In addition, according to Eq. (2), thermal conductivity includes three sections: electronic, lattice and bipolar thermal conductivity. Indeed, electronic thermal conductivity is defined by,

$$\kappa_e = L\sigma T, \tag{10}$$

where κ_e, L, σ and T refer to electronic thermal conductivity, Lorenz parameter, electrical conductivity and the absolute temperature respectively.[8] Lorenz parameter, electrical conductivity and the absolute temperature are on the order of 10^{-8} V^2/K^2, 10^5 S/m and 10^2 K respectively. As a result, electronic thermal conductivity is on the order of 10^{-1} W/(m·K), meanwhile lattice thermal conductivity is on the order of 10^0 W/(m·K), which indicates that a

high electronic thermal conductivity is not a problem when compared with the variation in lattice thermal conductivity. Furthermore, for the evaluation of ZT of Bi_2Te_3-based thermoelectric materials (especially ZT evaluation near room temperature), bipolar thermal conductivity can be ignored. As a result, effort should only be made on minimizing lattice thermal conductivity in order to reduce total thermal conductivity and consequently improve ZT of Bi_2Te_3-based solid solutions, which can be realized by introducing various phonon scattering mechanism into Bi_2Te_3-based alloy matrix.
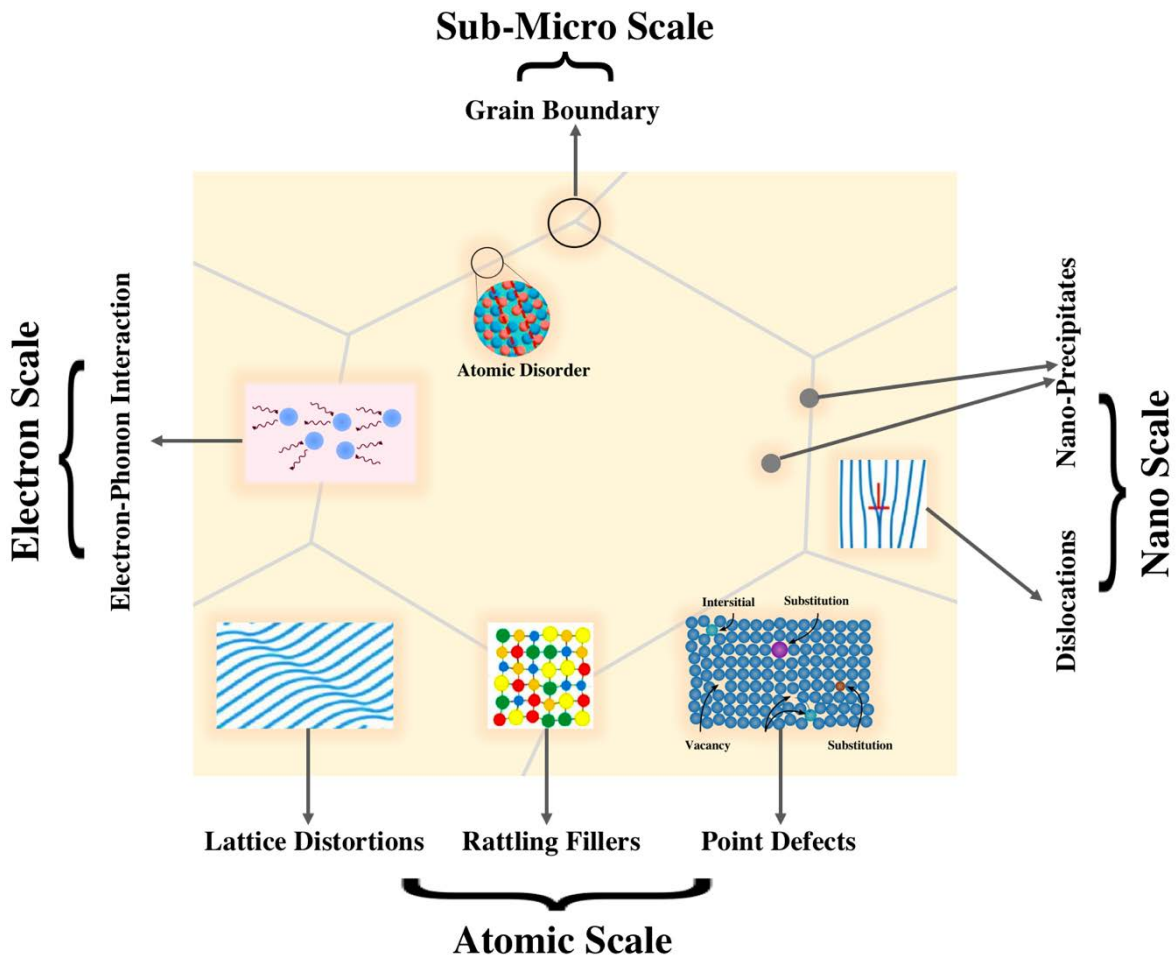
Figure 23. Various possible scattering centers for phonons.[8]

As shown in Fig. 23, in theory, different scattering centers from sub-micro, nano, atomic and electron scales can be introduced into Bi_2Te_3-based thermoelectric materials to optimize phonon scattering and consequently suppress lattice thermal conductivity. On the electron scale, interaction between electrons and phonons contributes to increase phonon scattering and reduce lattice thermal conductivity. For example, Liao et al. and Zhu et al. have reported analogous

reduction in lattice thermal conductivity of silicon which is attributed to the effect of electron-phonon interaction.[113,114] However, there is not any research attention that has been paid to the effect of interaction between electron and phonon on the thermoelectric performance of Bi_2Te_3-based alloys. On the atomic scale, rattling fillers can be introduced into thermoelectric materials with open structures to effectively suppress their lattice thermal conductivity. For example, considerably reduced lattice thermal conductivities of approximately 0.5 W/(m·K) and 1 W/(m·K) near room temperature are obtained through introducing different rattling fillers into skutterudites,[115,116] and these reduced lattice thermal conductivities almost reach the glass limit. However, up to date, few research work has been performed to study the relationship between rattling filler scattering and the lattice thermal conductivity of Bi_2Te_3 and its alloys. Atom-scale point defects (including interstitial, chemical substitution and vacancy), which have a length scale of phonons, can efficiently scatter phonons and suppress lattice thermal conductivity,[90,117,118] but these point effects will simultaneously have negative effects on electrical conductivity which cause a conflict between phonon and carrier transport properties. On the nano scale, phonon scattering from dislocations is efficient to minimize lattice thermal conductivity, and dislocations can be created by deformation of Bi_2Te_3-based thermoelectric materials during manufacture. For instance, Kim et al. have reported a noticeable decrease in lattice thermal conductivity through increasing the dislocation concentration in $Bi_{0.5}Sb_{1.5}Te_{3.0}$.[119] In short, for Bi_2Te_3-based thermoelectric materials, only grain boundaries, nano-precipitates and atomic disorder at grain boundary can serve as practical phonon scattering centers to suppress their lattice thermal conductivity, especially increased phonon scattering at grain boundaries which can be realized by nanostructuring engineering.

Over the last decade, nanostructuring engineering has been extensively applied to improve *ZT* of Bi_2Te_3-based thermoelectric materials because nanostructuring can cause increased grain boundary density (decreased grain sizes) or increased nano-precipitate concentration in Bi_2Te_3-based solutions, which strengthens phonon scattering and thus reduces lattice thermal conductivity.[120-123] In addition, as mentioned in Chapter 3, high-energy ball milling combined with compacting techniques (such as spark plasma sintering, hot-pressing and extrusion method) is frequently used to prepare nanostructured Bi_2Te_3-based materials. Indeed, grain

boundary phonon scattering mainly contributes to lattice thermal conductivity reduction at low temperatures, meanwhile lattice thermal conductivity can also have a considerable reduction at high temperature,[124] which mainly results from phonon scattering from atomic disorders at grain boundaries.
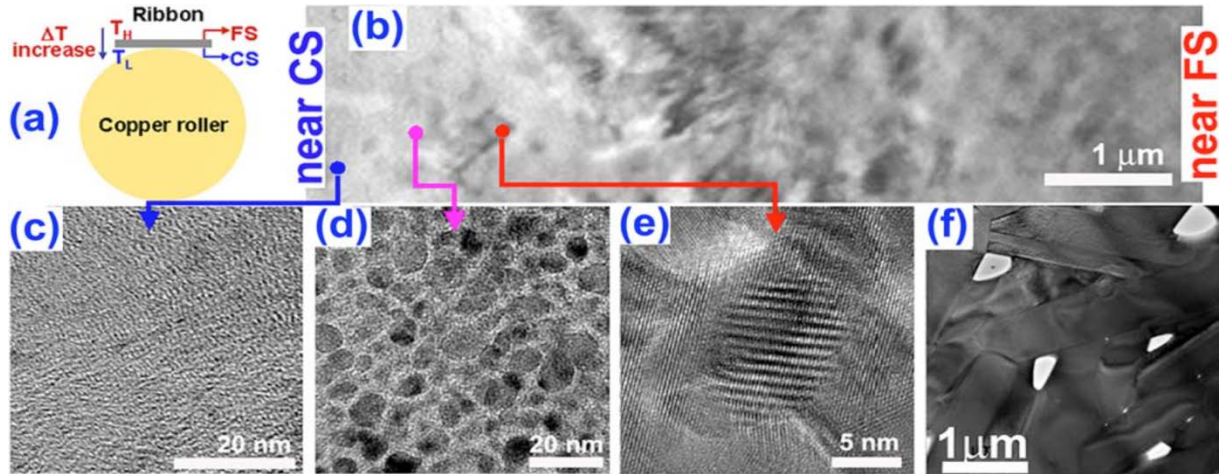
Figure 24. (a) Illustration of MS procedure, (b)-(e) transmission electron microscopy (TEM) images of cross section of $Bi_{0.52}Sb_{1.48}Te_3$ prepared by MS-SPS, (f) TEM images of free surface of $Bi_{0.52}Sb_{1.48}Te_3$ prepared by MS-SPS.[125]
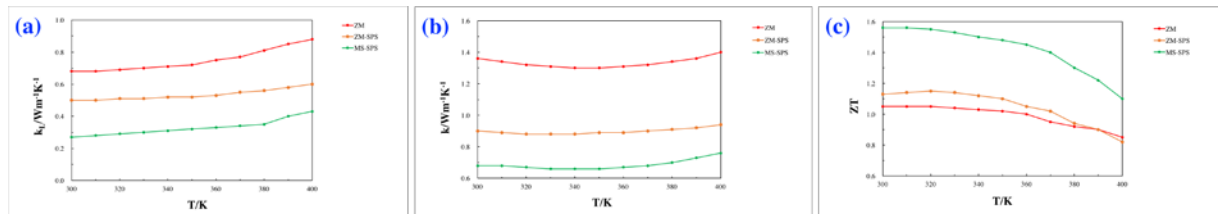
Figure 25. (a) Lattice thermal conductivity, (b) total thermal conductivity and (c) ZT of $Bi_{0.52}Sb_{1.48}Te_3$ prepared by ZM (red lines), ZM-SPS (yellow lines) and MS-SPS (green lines).[125]

In order to maximally suppress the thermal conductivity and thus improve ZT values of Bi_2Te_3-based materials, the use of nanostructure engineering and the use of increased grain boundary phonon scattering have been extensively reported, such as ZT_{max} = 1.4 at 373 K of nanocrystalline $Bi_{0.5}Sb_{1.5}Te_3$,[76] ZT_{max} = 1.3 at 348 K of nanocrystalline $Bi_xSb_{2-x}Te_3$,[75] and ZT_{max} = 1.46 at 443 K of nanostructured $BiSbTe_3$[126]. However, a more successful example of nanostructured Bi_2Te_3-based thermoelectric materials with low thermal conductivity and resultant high ZT is MS-SPS $Bi_{0.52}Sb_{1.48}Te_3$ which is prepared from zone melted (ZM) $Bi_{0.52}Sb_{1.48}Te_3$ ingots through melt spinning (MS) followed by spark plasma sintering (SPS).[125]

In the experimental work, MS procedure is performed according to Fig. 24(a), and thus there is a temperature difference between free surface (FS) and contact surface (CS). The temperature difference between CS and FS leads to the crystallization difference, which results in different micromorphology (shown in Fig. 24(b)-(f)). It can be noticed that micromorphology of MS-SPS $Bi_{0.52}Sb_{1.48}Te_3$ is dependent on the position relative to the copper roller. The phase is amorphous near CS (shown in Fig. 24(c)), meanwhile the phase is nanocrystalline near FS (shown in Fig. 24(f)). As a result, MS-SPS $Bi_{0.52}Sb_{1.48}Te_3$ possesses special microstructures with nanocrystalline domains in amorphous matrix. In order to deeply understand the effect of MS technique or special microstructures with nanocrystalline domains in amorphous matrix on improving thermoelectric performance of $Bi_{0.52}Sb_{1.48}Te_3$, Figure 25(a)-(c) compare the lattice thermal conductivity, total thermal conductivity and ZT values of ZM $Bi_{0.52}Sb_{1.48}Te_3$ ingots, ZM-SPS $Bi_{0.52}Sb_{1.48}Te_3$ (Zone melted $Bi_{0.52}Sb_{1.48}Te_3$ ingots are firstly milled into 100-μm powers and then compacted into bulk materials by SPS) and MS-SPS $Bi_{0.52}Sb_{1.48}Te_3$. MS-SPS samples exhibit the lowest lattice thermal conductivity (shown in Fig. 25(a)) and thus the lowest total thermal conductivity (shown in Fig. 25(b)), which is attributed to the increased grain boundary phonon scattering as there are nano grains (nano crystals) in MS-SPS $Bi_{0.52}Sb_{1.48}Te_3$. Furthermore, due to the special microstructures which consists of nanocrystalline domains in amorphous matrix, electrical properties (electrical conductivity, Seebeck coefficient and power factor) have not been affected and thus still remain at a high level. As a result, thermoelectric performance of $Bi_{0.52}Sb_{1.48}Te_3$ has been considerably improved, and MS-SPS $Bi_{0.52}Sb_{1.48}Te_3$ exhibit the highest ZT value of 1.56 at 300 K, resulting from significant lattice thermal conductivity reduction but unaffected electrical properties, and similar results have been also reported by Xie et al. and Tang et al..[127,128]

In addition to optimized phonon scattering at grain boundary, nanoporous Bi_2Te_3-based thermoelectric materials can also experience a reduction in lattice thermal conductivity and thus an increase in ZT values due to increased phonon scattering at nanopore sites. For instance, Zhang et al. have reported that nanoporous Bi_2Te_3 with a porosity ratio of 3.32% exhibits a ZT
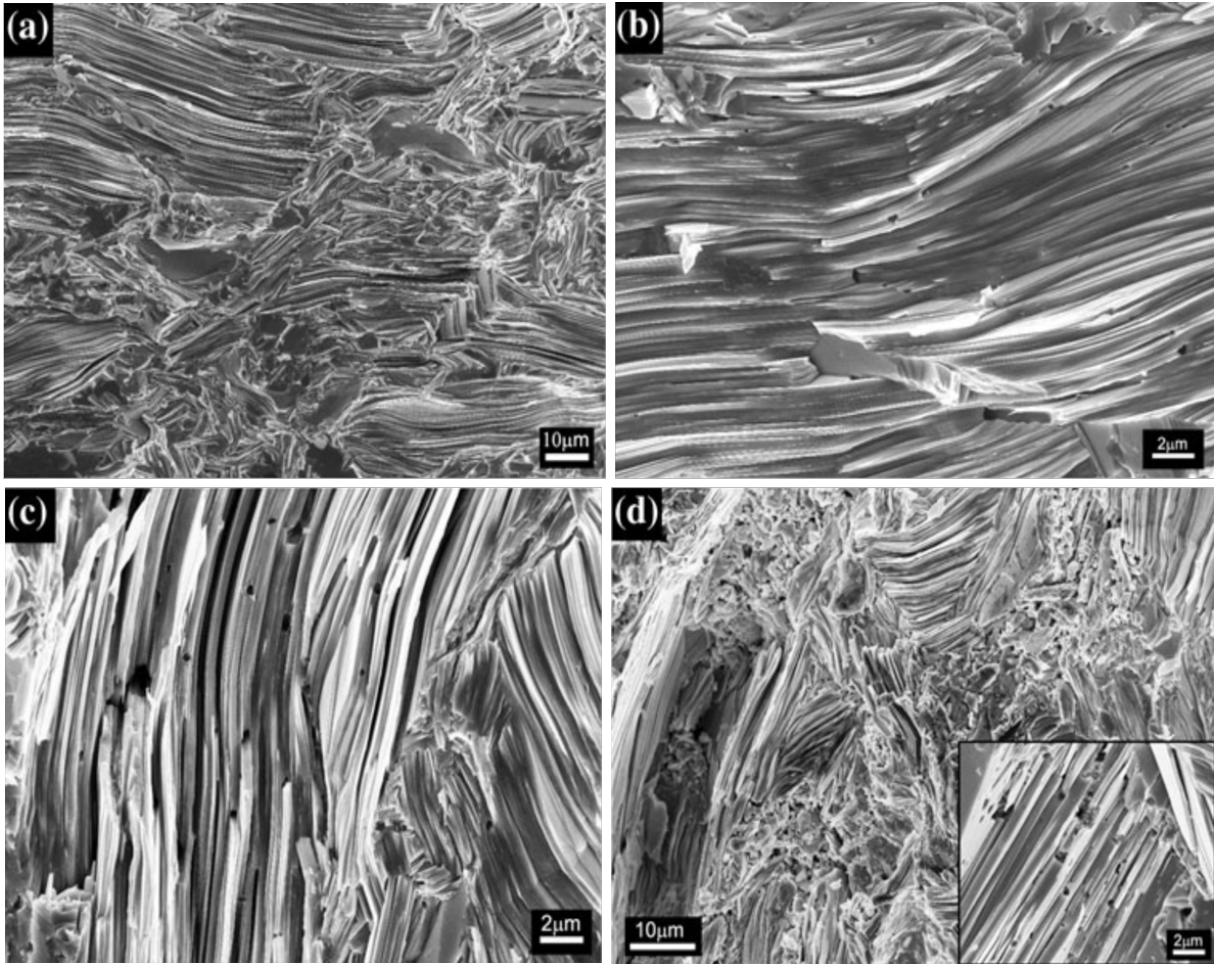
Figure 26. Field-emission scanning electron microscopy images of nanoporous Bi_2Te_3 with a porosity ratio of (a) 0%, (b) 1.81%, (c) 3.32%, and (d) 4.46%.[129]
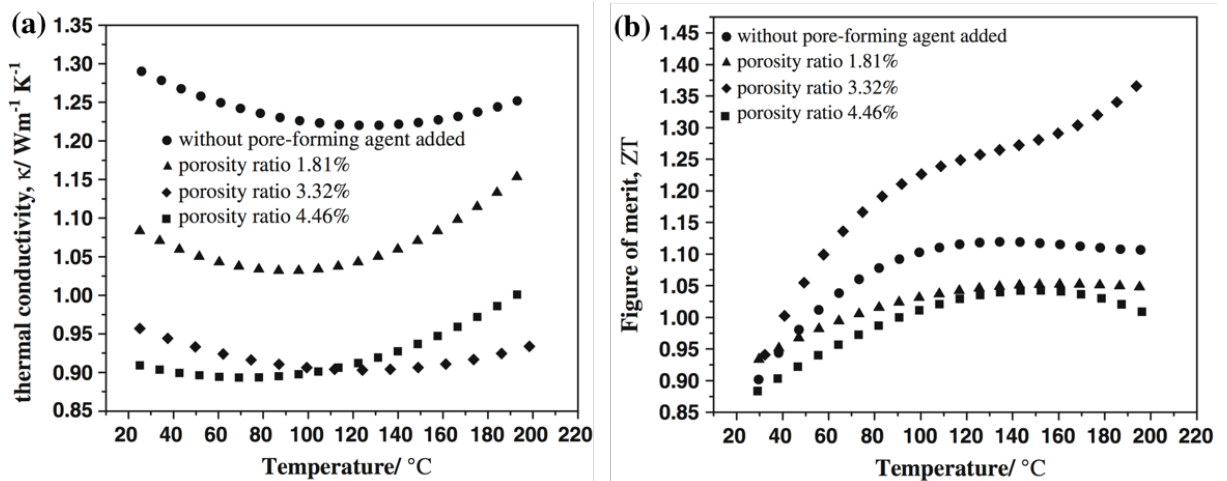
Figure 27. (a) Thermal conductivity and (b) *ZT* of nanoporous Bi_2Te_3 with different porosity ratio.[129]

as high as 1.38 at 473 K.[129] Figure 26(a)-(c) illustrate the morphology of nanoporous Bi_2Te_3 with different porosity ratio and indicate that these nanopores randomly distribute in Bi_2Te_3. These randomly distributed nanopores serve as phonon scattering centres and thus lattice thermal conductivity can be reduced. Figure 27(a) shows that thermal conductivity of nanoporous Bi_2Te_3 is extremely low (especially when porosity ratio reaches 3.32%) when compared with Bi_2Te_3 without nanopores. This result can be explained by decreased lattice thermal conductivity induced by phonon blocking from nanopores. In addition, there is only a small difference between thermal conductivities of nanoporous Bi_2Te_3 with a porosity ratio of 3.32% and 4.46%. Therefore, a moderate porosity ratio should be selected to ensure high *ZT* values and simultaneously maintain good mechanical properties. Furthermore, there is a slight increase in Seebeck coefficient but a small decrease in electrical conductivity, which leads to an almost unaffected power factor. As a result, the introduction of nanopores into Bi_2Te_3-based materials can effectively enhance the *ZT* values (shown in Fig. 27(b)), and nanoporous Bi_2Te_3 with a porosity ratio of 3.32% can obtain a maximum *ZT* of 1.38 at 473 K. Since nanopores can be used to suppress lattice thermal conductivity, increased grain boundary phonon scattering can be combined with nanoporous structures in Bi_2Te_3-based materials in order to further suppress lattice thermal conductivity of Bi_2Te_3 and its alloys.[130-132]

To summarize, total thermal conductivity reduction is mainly dependent on lattice thermal conductivity reduction that can be realized by strengthened phonon scattering, and nanostructuring engineering, nanoporous structures or the combination of both can be used to strengthen phonon scattering in Bi_2Te_3-based thermoelectric materials. Importantly, the combination of melting spinning and spark plasma sintering can result in obtaining special microstructures in Bi_2Te_3-based thermoelectric materials. These special microstructures include nanocrystalline domains in the amorphous matrix, which leads to reduced lattice thermal conductivity but ensuring high power factor unaffected. As a result, thermoelectric performance can be maximally improved. However, since lattice thermal conductivity reduction is crucial to enhance thermoelectric performance of Bi_2Te_3-based materials, other phonon scattering mechanisms (described in Fig. 23) should also be applied to Bi_2Te_3-based materials, and thus lattice thermal conductivity can be further suppressed. Therefore, the future

research work should focus more on applying these phonon scattering mechanisms to Bi_2Te_3-based materials.

5.   Conclusion

The objective of this thesis was to review Bi_2Te_3-based thermoelectric materials. Layered Bi_2Te_3 exhibits a narrow band gap, which enables it to be a good thermoelectric material. In addition, Bi_2Te_3 shows anisotropic structure and thermoelectric properties, which are thermoelectrically favourable. Furthermore, Sb_2Te_3 and Bi_2Se_3 share the same crystal structure as well as electronic structure with Bi_2Te_3. Therefore, formed homogeneous solid solutions $Bi_xSb_{2-x}Te_3$ and $Bi_2Te_{3-y}Se_y$ also share the same crystal structure as well as electronic structure with Bi_2Te_3. Antisite defects Bi'_{Te} and/or Sb'_{Te} in $Bi_xSb_{2-x}Te_3$ contribute to increased concentration of hole $h^{\cdot}$, and thus antisite defects can be used to tune electric conductivity of Bi_2Te_3-based thermoelectric materials. The addition of Se results in strengthened alloy scattering for both carriers and phonons, and thus Bi_2Te_3 should be alloyed with an appropriate amount of Se to achieve balance between carrier and phonon transport properties.

With regard to synthesis processes, this thesis has reviewed six typical ones that are simple and cost-efficiency because they use simple starting materials and fabrication machines.

- Solvothermal/hydrothermal method is mainly used to produce nanostructured Bi_2Te_3-based thermoelectric materials and follows a typical process: preparation of precursor solution, high-temperature synthetic reaction, cooling and collection. Constant stirring during high-temperature synthetic reaction contributes to high phase purity, meanwhile the use of glucose and/or NaOH helps to control the morphology.

- Magnetron sputtering is mainly used to fabricate Bi_2Te_3-based thin films. For the application of this synthesis method, several key points should be considered: (1) sputtering target should be individual elements; (2) substrates should remain cool and be rotated; (3) low sputtering power should be selected; and (4) EB irradiation and thermal annealing help to obtain high-performance Bi_2Te_3-based thin films.

- Thermal evaporation is mainly used to produce Bi_2Te_3-based thin films, and substrate temperature greatly affects crystalline structure of films.

- Flash evaporation is a thin-film technique which is similar to thermal evaporation. The

appropriate distance between evaporation source and substrate is 200 mm to produce Bi_2Te_3-based thin films with clean surface. In addition, annealing and sintering help to enhance crystallinity of Bi_2Te_3-based thin films.

- Electrochemical deposition can prepare Bi_2Te_3-based thick films and nanowires. In this method, the use of low-concentration electrolytes contributes to obtaining high-crystallinity Bi_2Te_3-based thermoelectric materials.

- High-energy ball milling can manufacture bulk and nanostructured Bi_2Te_3-based thermoelectric materials which tend to exhibit high-thermoelectric performance because of thermal conductivity reduction.

With regard to thermoelectric performance improvement of Bi_2Te_3-based materials, three strategies are reviewed: electrical conductivity improvement (enhancing carrier concentration and mobility), Seebeck coefficient improvement and thermal conductivity reduction.

- Optimizing carrier concentration can be realized by doping and increasing antisite defect concentration in Bi_2Te_3-based thermoelectric materials, and hydrogen annealing as well as addition of Sb can be employed to increase antisite defects.

- Optimizing carrier mobility can be realized by reconstructing random grain boundaries (crystal lattice) which results in suppressing carrier scattering at grain boundaries.

- Optimizing Seebeck coefficient can be realized by the use of high pressure sintering techniques which can result in high energy barrier concentration in Bi_2Te_3-based thermoelectric materials.

- Thermal conductivity reduction can be realized by the use of nanostructuring engineering, nanoporous structures or the combination of both which results in strengthened phonon scattering. Importantly, the combination of melting spinning and spark plasma sintering can not only result in reduced lattice thermal conductivity but also ensuring high power factor unaffected.

There are still many challenges related to Bi_2Te_3-based thermoelectric materials, although these materials have been extensively researched. For example, during synthesis processes, it is a big

challenge to ensure the accurate stoichiometry. In addition, improving *ZT* values to 2 is challenging due to the conflicts among thermoelectric parameters. Based on these current challenges and previous literature review, some suggestions are made here. Firstly, using individual elements as starting materials may be the potential solution to ensuring accurate stoichiometry. Secondly, decoupling the interactions among thermoelectric parameters is suggested to further improve *ZT*. Thirdly, in order to obtain high-purity products, it is suggested to control the chemical reaction rates in solvothermal/hydrothermal method and electrochemical deposition. Fourthly, since morphology significantly affects thermoelectric efficiency, future research work should attach emphasis on identifying and producing desired morphology. Finally, in magnetron sputtering, thermal and flash evaporation, since the substrates are suggested to remain cool which cannot trigger crystallization of products, a possible research opportunity is related to discovery substrates that can directly trigger crystal growth.

Overall, this thesis has comprehensively reviewed Bi_2Te_3-based thermoelectric materials. Many current challenges, possible research opportunities and recommendations have been presented. Therefore, this thesis could offer a deep understanding of Bi_2Te_3-based thermoelectric materials and possibly guide future research.

References

1   Avni, A. & Blázquez, M. A. Can Plant Biotechnology Help in Solving Our Food and Energy Shortage in the Future? *Current Opinion in Biotechnology* **22**, 220-223, doi:10.1016/j.copbio.2011.01.007 (2011).

2   United States: International Energy Outlook 2016. (Bangkok, 2016).

3   Szczech, J. R., Higgins, J. M. & Jin, S. Enhancement of the Thermoelectric Properties in Nanoscale and Nanostructured Materials. *Journal of Materials Chemistry* **21**, 4037-4055, doi:10.1039/c0jm02755c (2011).

4   Li, J. F., Liu, W. S., Zhao, L. D. & Zhou, M. High-Performance Nanostructured Thermoelectric Materials. *NPG Asia Materials* **2**, 152-158, doi:10.1038/asiamat.2010.138 (2010).

5   *Thermoelectric Generator Picture*, <https://www.google.com.au/search?q=thermoelectric+generator&source=lnms&tbm=isch&sa=X&ved=0ahUKEwia9Mzy0-fVAhUBxLwKHe_uA0AQ_AUICigB&biw=1280&bih=716 -imgrc=Y0h9bQQHWnVBVM:> (

6   Xu, H. *et al.* Electrical Transport Properties of Microwave-Synthesized $Bi_2Se_{3-x}Te_x$ Nanosheet. *CrystEngComm* **15**, 5626-5632, doi:10.1039/c3ce40296g (2013).

7   Sootsman, J. R., Chung, D. Y. & Kanatzidis, M. G. New and Old Concepts in Thermoelectric Materials. *Angew. Chem. Int. Ed,* **48**, 8616-8639, doi:10.1002/anie.200900598 (2009).

8   Zhu, T. *et al.* Compromise and Synergy in High-Efficiency Thermoelectric Materials. *Advanced Materials* **29(14)**, 1-26, doi:10.1002/adma.201605884 (2017).

9   Heremans, J. P. *et al.* Enhancement of Thermoelectric Efficiency in PbTe by Distortion of the Electronic Density of States. *Science* **321**, 554-557, doi:10.1126/science.1159725 (2008).

10   Zhu, G. H. *et al.* Increased Phonon Scattering by Nanograins and Point Defects in Nanostructured Silicon with a Low Concentration of Germanium. *Physical Review Letters* **102(196803)**, 1-4, doi:10.1103/PhysRevLett.102.196803 (2009).

11   Nolas, G. S., Sharp, J. & Goldsmid, H. J. *Thermoelectrics Basic Principles and New Materials Developments*. (Berlin, Heidelberg : Springer Berlin Heidelberg : Imprint: Springer, 2001).

12   Radhakrishnan, R. A Review of: " Thermoelectric Handbook, Macro to Nano, D.M. Rowe (Editor)". **23**, 626-627, doi:10.1080/10426910802135819 (2008).

13   Guo, X. *et al.* Thermoelectric Transport Properties and Crystal Growth of $BiSbTe_3$ Bulk Materials Produced by a Unique High-Pressure Synthesis. *CrystEngComm* **15**, 7236-7242, doi:10.1039/c3ce40780b (2013).

14   Rama, V., Edward, S., Thomas, C., Brooks, O. & Quinn. Thin-Film Thermoelectric Devices with High Room-Temperature Figures of Merit. *Nature* **413**, 597-602, doi:10.1038/35098012 (2001).

15   Eibl, O., Nielsch, K., Peranio, N. & Völklein, F. *Thermoelectric Bi_2Te_3 Nanomaterials*. (Hoboken : Wiley, 2015).

16   Wiese, J. R. & Muldawer, L. Lattice Constants of Bi_2Te_3-Bi_2Se_3 Solid Solution Alloys. *Journal of Physics and Chemistry of Solids* **15**, 13-16, doi:10.1016/0022-3697(60)90094-9 (1960).

17   *Crystal Structure Model of Bi2Te3*, <https://www.google.com.au/search?q=Crystal+Structure+Model+of+Bi2Te3&source=lnms&tbm=isch&sa=X&ved=0ahUKEwi1_52l8OrVAhWKa7wKHd0UBDQQ_AUICigB&biw=1280&bih=716 - imgrc=7pUrb7zEL7BXjM:> (

18   Huang, B. L. & Kaviany, M. Ab Initio and Molecular Dynamics Predictions for Electron and Phonon Transport in Bismuth Telluride. *Physical Review B - Condensed Matter and Materials Physics* **77**, 1-19, doi:10.1103/PhysRevB.77.125209 (2008).

19   Yamauchi, K. & Takashiri, M. Highly Oriented Crystal Growth of Nanocrystalline Bismuth Telluride Thin Films with Anisotropic Thermoelectric Properties Using Two-Step Treatment. *Journal of Alloys and Compounds* **698**, 977-983, doi:10.1016/j.jallcom.2016.12.284 (2017).

20   Jacquot, A. *et al.* Thermoelectric Properties as a Function of Electronic Band Structure and Microstructure of Textured Materials. *Journal of Electronic Materials* **39**, 1861-1868, doi:10.1007/s11664-009-1059-x (2010).

21   Nakajima, S. The Crystal Structure of $Bi_2Te_{3-X}Se_x$. *Journal of Physics and Chemistry of Solids* **24**, 479-485, doi:10.1016/0022-3697(63)90207-5 (1963).

22   Francombe, M. H. Structure-Cell Data and Expansion Coefficients of Bismuth Telluride. *British Journal of Applied Physics* **9**, 415-417, doi:10.1088/0508-3443/9/10/307 (1958).

23   Cheng, L. *et al.* Effects of Van Der Waals Interactions and Quasiparticle Corrections on the Electronic and Transport Properties of Bi_2Te_3. *Physical Review B - Condensed Matter and Materials Physics* **90(085118)**, 1-17, doi:10.1103/PhysRevB.90.085118 (2014).

24   Arora, S., Jaimini, V., Srivastava, S. & Vijay, Y. K. Properties of Nanostructure Bismuth Telluride Thin Films Using Thermal Evaporation. *Journal of Nanotechnology* **4276506**, 1-4 (2017).

25   Noh, H. J. *et al.* Spin-Orbit Interaction Effect in the Electronic Structure of Bi_2Te_3 Observed by Angle-Resolved Photoemission Spectroscopy. *EPL (Europhysics Letters)* **81(57006)**, 1-5 doi:10.1209/0295-5075/81/57006 (2008).

26   Park, M. S. *et al.* Electronic Structure and Volume Effect on Thermoelectric Transport in p-Type Bi and Sb Tellurides. *Phys. Rev. B* **81(155211)**, 1-5, doi:10.1103/PhysRevB.81.155211 (2010).

27   Kim, M., Freeman, A. J. & Geller, C. B. Screened Exchange LDA Determination of the Ground and Excited State Properties of Thermoelectrics: Bi_2Te_3. *Physical Review B - Condensed Matter and Materials Physics* **72**, 1-4, doi:10.1103/PhysRevB.72.035205 (2005).

28   Anderson, T. & Krause, H. Refinement of the Sb_2Te_3 and Sb_2Te_2Se Structures and Their Relationship to Nonstoichiometric $Sb_2Te_{3-y}Se_y$ Compounds. *Acta Cryst* **b30**, 1307-1310 (1974).

29   Wang, G. & Cagin, T. Electronic Structure of the Thermoelectric Materials Bi_2Te_3 and Sb_2Te_3 from First-Principles Calculations. *Physical Review B - Condensed Matter and Materials Physics* **76**, 1-8, doi:10.1103/PhysRevB.76.075201 (2007).

30   Zhao, L. D., Zhang, B. P., Liu, W. S., Zhang, H. L. & Li, J. F. Effects of Annealing on Electrical Properties of n-Type Bi_2Te_3 Fabricated by Mechanical Alloying and Spark

Plasma Sintering. *Journal of Alloys and Compounds* **467**, 91-97, doi:10.1016/j.jallcom.2007.12.063 (2009).

31   Son, J. *et al.* Effect of Ball Milling Time on the Thermoelectric Properties of p-Type $(Bi,Sb)_2Te_3$. *Journal of Alloys and Compounds* **566**, 168-174, doi:10.1016/j.jallcom.2013.03.062 (2013).

32   Seo, S., Jeong, Y., Oh, M.-W. & Yoo, B. Effect of Hydrogen Annealing of Ball-Milled $Bi_{0.5}Sb_{1.5}Te_3$ Powders on Thermoelectric Properties. *Journal of Alloys and Compounds* **706**, 576-583, doi:10.1016/j.jallcom.2017.02.181 (2017).

33   Eum, A. Y. *et al.* Thermoelectric and Transport Properties of Mechanically-Alloyed $Bi_2Te_{3-y}Se_y$ Solid Solutions. *Journal of the Korean Physical Society* **67**, 1809-1813, doi:10.3938/jkps.67.1809 (2015).

34   Liang, Y. *et al.* Influence of NaOH on the Formation and Morphology of Bi_2Te_3 Nanostructures in a Solvothermal Process: from Hexagonal Nanoplates to Nanorings. *Materials Chemistry and Physics* **129**, 90-98, doi:10.1016/j.matchemphys.2011.03.061 (2011).

35   Zhang, G., Wang, W., Lu, X. & Li, X. Solvothermal Synthesis of V-VI Binary and Ternary Hexagonal Platelets: the Oriented Attachment Mechanism. *Crystal Growth and Design* **9**, 145-150, doi:10.1021/cg7012528 (2009).

36   Song, S., Fu, J., Li, X., Gao, W. & Zhang, H. Facile Synthesis and Thermoelectric Properties of Self-Assembled Bi_2Te_3 One-Dimensional Nanorod Bundles. *Chemistry – A European Journal* **19**, 2889-2894, doi:10.1002/chem.201203437 (2013).

37   Jiang, L., Zhu, Y. J. & Cui, J. B. Nanostructures of Metal Tellurides (PbTe, CdTe, $CoTe_2$, Bi_2Te_3, and Cu_7Te_4) with Various Morphologies: A General Solvothermal Synthesis and Optical Properties. *Eur. J. Inorg. Chem,* **2010**, 3005-3011, doi:10.1002/ejic.201000251 (2010).

38   Takashiri, M., Kai, S., Wada, K., Takasugi, S. & Tomita, K. Role of Stirring Assist during Solvothermal Synthesis for Preparing Single-Crystal Bismuth Telluride Hexagonal Nanoplates. *Materials Chemistry and Physics* **173**, 213-218, doi:10.1016/j.matchemphys.2016.02.007 (2016).

39   Peranio, N., Leister, E., Töllner, W., Eibl, O. & Nielsch, K. Stoichiometry Controlled, Single-Crystalline Bi_2Te_3 Nanowires for Transport in the Basal Plane. *Advanced Functional Materials* **22**, 151-156, doi:10.1002/adfm.201101273 (2012).

40   Zhang, G., Yu, Q., Wang, W. & Li, X. Nanostructures for Thermoelectric Applications: Synthesis, Growth Mechanism, and Property Studies. *Advanced Materials* **22**, 1959-1962, doi:10.1002/adma.200903812 (2010).

41   Zhang, G., Yu, Q., Yao, Z. & Li, X. Large Scale Highly Crystalline Bi_2Te_3 Nanotubes through Solution Phase Nanoscale Kirkendall Effect Fabrication. *Chemical Communications*, 2317-2319, doi:10.1039/b822595h (2009).

42   Jin, R., Liu, J. & Li, G. Facile Solvothermal Synthesis, Growth Mechanism and Thermoelectric Property of Flower-Like Bi_2Te_3. *Crystal Research and Technology* **49**, 460-466, doi:10.1002/crat.201400012 (2014).

43   Takashiri, M. *et al.* Effect of Grain Size on Thermoelectric Properties of n-Type Nanocrystalline Bismuth-Telluride Based Thin Films. *Journal of Applied Physics* **104(084302)**, 1-6, doi:10.1063/1.2990774 (2008).

44   Fang, B., Zeng, Z., Yan, X. & Hu, Z. Effects of Annealing on Thermoelectric Properties of Sb_2Te_3 Thin Films Prepared by Radio Frequency Magnetron Sputtering. *Journal of Materials Science: Materials in Electronics* **24**, 1105-1111, doi:10.1007/s10854-012-0888-1 (2013).

45   Bourgault, D., Garampon, C. G., Caillault, N., Carbone, L. & Aymami, J. A. Thermoelectric Properties of n-Type $Bi_2Te_{2.7}Se_{0.3}$ and p-Type $Bi_{0.5}Sb_{1.5}Te_3$ Thin Films Deposited by Direct Current Magnetron Sputtering. *Thin Solid Films* **516**, 8579-8583, doi:10.1016/j.tsf.2008.06.001 (2008).

46   Huang, H., Luan, W.-L. & Tu, S.-T. Influence of Annealing on Thermoelectric Properties of Bismuth Telluride Films Grown via Radio Frequency Magnetron Sputtering. *Thin Solid Films* **517**, 3731-3734, doi:10.1016/j.tsf.2009.01.015 (2009).

47   Kusagaya, K., Hagino, H., Tanaka, S., Miyazaki, K. & Takashiri, M. Structural and Thermoelectric Properties of Nanocrystalline Bismuth Telluride Thin Films under Compressive and Tensile Strain. *Journal of Electronic Materials* **44**, 1632-1636, doi:10.1007/s11664-014-3496-4 (2015).

48   Kusagaya, K. & Takashiri, M. Investigation of the Effects of Compressive and Tensile Strain on n-Type Bismuth Telluride and p-Type Antimony Telluride Nanocrystalline Thin Films for Use in Flexible Thermoelectric Generators. *Journal of Alloys and Compounds* **653**, 480-485, doi:10.1016/j.jallcom.2015.09.039 (2015).

49   Lin, H.-J. *et al.* Effect of Annealing Temperature on the Thermoelectric Properties of the $Bi_{0.5}Sb_{1.5}Te_3$ Thin Films Prepared by Radio-Frequency Sputtering. *Metallurgical and Materials Transactions A* **44**, 2339-2345, doi:10.1007/s11661-012-1587-5 (2013).

50   Takashiri, M., Asai, Y. & Yamauchi, K. Structural, Optical, and Transport Properties of Nanocrystalline Bismuth Telluride Thin Films Treated with Homogeneous Electron Beam Irradiation and Thermal Annealing. *Nanotechnology* **27(335703)**, 1-7, doi:10.1088/0957-4484/27/33/335703 (2016).

51   Lin, J. M., Chen, Y. C., Yang, C. F. & Chen, W. Effect of Substrate Temperature on the Thermoelectric Properties of the SbTe Thin Films Deposition by Using Thermal Evaporation Method. *Journal of Nanomaterials* **2015(135130)**, 1-6, doi:10.1155/2015/135130 (2015).

52   Lin, J. M., Chen, Y. C. & Chen, W. Influence of Deposition Rate on the Thermoelectric Properties of SbTe Thin Films by Thermal Evaporation Method. *Journal of Nanomaterials* **2015(564954)**, 1-5, doi:10.1155/2015/564954 (2015).

53   Lin, J. M., Chen, Y. C. & Lin, C. P. Annealing Effect on the Thermoelectric Properties of BiTe Thin Films Prepared by Thermal Evaporation Method. *Journal of Nanomaterials* **2013(201017)**, 1-6, doi:10.1155/2013/201017 (2013).

54   Takashiri, M., Shirakawa, T., Miyazaki, K. & Tsukamoto, H. Fabrication and Characterization of $Bi_{0.4}Te_{3.0}Sb_{1.6}$ Thin Films by Flash Evaporation Method. *Journal of Alloys and Compounds* **441**, 246-250, doi:10.1016/j.jallcom.2006.09.136 (2007).

55   Takashiri, M., Miyazaki, K. & Tsukamoto, H. Structural and Thermoelectric Properties of Fine-Grained $Bi_{0.4}Te_{3.0}Sb_{1.6}$ Thin Films with Preferred Orientation Deposited by Flash Evaporation Method. *Thin Solid Films* **516**, 6336-6343, doi:10.1016/j.tsf.2007.12.130 (2008).

56   Takashiri, M., Tanaka, S. & Miyazaki, K. Determination of the Origin of Crystal Orientation for Nanocrystalline Bismuth Telluride-Based Thin Films Prepared by Use

of the Flash Evaporation Method.(Author abstract). *Journal of Electronic Materials* **43**, 1881-1889, doi:10.1007/s11664-013-2896-1 (2014).

57   Takashiri, M., Tanaka, S., Hagino, H. & Miyazaki, K. Strain and Grain Size Effects on Thermal Transport in Highly-Oriented Nanocrystalline Bismuth Antimony Telluride Thin Films. *International Journal of Heat and Mass Transfer* **76**, 376-384, doi:10.1016/j.ijheatmasstransfer.2014.04.048 (2014).

58   Erdoğan, İ. Y. & Demir, Ü. Synthesis and Characterization of Sb_2Te_3 Nanofilms via Electrochemical Co-Deposition Method. *Journal of Electroanalytical Chemistry* **633**, 253-258, doi:10.1016/j.jelechem.2009.06.010 (2009).

59   Manzano, C. *et al.* Thermoelectric Properties of Bi_2Te_3 Films by Constant and Pulsed Electrodeposition. *Current Research and Development in Science and Technology* **17**, 2071-2078, doi:10.1007/s10008-013-2066-7 (2013).

60   Trung, N. H., Sakamoto, K., Toan, N. V. & Ono, T. Synthesis and Evaluation of Thick Films of Electrochemically Deposited Bi_2Te_3 and Sb_2Te_3 Thermoelectric Materials. *Materials (Basel, Switzerland)* **10(154)**, 1-17, doi:10.3390/ma10020154 (2017).

61   Maas, M., Diliberto, S., Vaulx, C., Azzouz, K. & Boulanger, C. Use of a Soluble Anode in Electrodeposition of Thick Bismuth Telluride Layers. *Journal of Electronic Materials* **43**, 3857-3862, doi:10.1007/s11664-014-3292-1 (2014).

62   Wu, M. *et al.* Electrodeposition of Bismuth Telluride Thermoelectric Films from Chloride-Free Ethylene Glycol Solutions. *Journal of the Electrochemical Society* **160**, 196-201, doi:10.1149/2.089304jes (2013).

63   Lee, J. *et al.* Power Factor Measurements of Bismuth Telluride Nanowires Grown by Pulsed Electrodeposition. *Rapid Research Letters* **4**, 43-45, doi:10.1002/pssr.200903368 (2010).

64   Frantz, C., Stein, N., Gravier, L., Granville, S. & Boulanger, C. Electrodeposition and Characterization of Bismuth Telluride Nanowires. *Journal of Electronic Materials* **39**, 2043-2048, doi:10.1007/s11664-009-1001-2 (2010).

65   Frantz, C. *et al.* Electrodeposition of Bismuth Telluride Nanowires with Controlled Composition in Polycarbonate Membranes. *Electrochimica Acta* **69**, 30-37, doi:10.1016/j.electacta.2012.01.040 (2012).

66   Picht, O. *et al.* Tuning the Geometrical and Crystallographic Characteristics of Bi_2Te_3 Nanowires by Electrodeposition in Ion-Track Membranes. *Journal of Physical Chemistry C* **116**, 5367-5375, doi:10.1021/jp210491g (2012).

67   Chang, T. *et al.* Individual Thermoelectric Properties of Electrodeposited Bismuth Telluride Nanowires in Polycarbonate Membranes. *Electrochimica Acta* **161**, 403-407, doi:10.1016/j.electacta.2015.02.105 (2015).

68   Lan, Y. C., Minnich, A. J., Chen, G. & Ren, Z. F. Enhancement of Thermoelectric Figure-of-Merit by a Bulk Nanostructuring Approach. *Adv. Funct. Mater.* **20**, 357-376, doi:10.1002/adfm.200901512 (2010).

69   Guo, X. *et al.* Investigating the Thermoelectric Properties of Synthesized Bi_2Te_3 under Different Synthesis Pressures. *Chemical Physics Letters* **568-569**, 190-194, doi:10.1016/j.cplett.2013.03.027 (2013).

70   Yan, X. *et al.* Experimental Studies on Anisotropic Thermoelectric Properties and Structures of n-type $Bi_2Te_{2.7}Se_{0.3}$. *Nano Letters* **10**, 3373-3378, doi:10.1021/nl101156v (2010).

71   Lee, G.-E. *et al.* Process Controls for Bi_2Te_3-Sb_2Te_3 Prepared by Mechanical Alloying and Hot Pressing. *Journal of the Korean Physical Society* **65**, 2066-2070, doi:10.3938/jkps.65.2066 (2014).

72   Lee, G.-E. *et al.* Thermoelectric Properties of Bi_2Te_3-Bi_2Se_3 Solid Solutions Prepared by Attrition Milling and Hot Pressing. *Journal of the Korean Physical Society* **65**, 1908-1912, doi:10.3938/jkps.65.1908 (2014).

73   Drabkin, I. A. *et al.* Structure and Thermoelectric Properties of Nanostructured $(Bi,Sb)_2Te_3$ (Review). *Advances in Materials Physics and Chemistry* **3**, 119-132 (2013).

74   Eum, A. Y. *et al.* Thermoelectric Properties of $Bi_2Te_{3-y}Se_y$:I_m Prepared by Mechanical Alloying and Hot Pressing. *Journal of Electronic Materials* **46**, 2623-2628, doi:10.1007/s11664-016-4828-3 (2017).

75   Ma, Y. *et al.* Enhanced Thermoelectric Figure-of-Merit in p-Type Nanostructured Bismuth Antimony Tellurium Alloys Made from Elemental Chunks. *Nano letters* **8**, 2580-2584, doi:10.1021/nl8009928 (2008).

76 Poudel, B. *et al.* High-Thermoelectric Performance of Nanostructured Bismuth Antimony Telluride Bulk Alloys. *Science* **320**, 634-638, doi:10.1126/science.1156446 (2008).

77 Joseph, P. H., Mildred, S. D., Lon, E. B. & Donald, T. M. When Thermoelectrics Reached the Nanoscale. *Nature Nanotechnology* **8**, 471-473, doi:10.1038/nnano.2013.129 (2013).

78 Dresselhaus, M. S. *et al.* New Directions for Low-Dimensional Thermoelectric Materials. *Advanced Materials* **19**, 1043-1053, doi:10.1002/adma.200600527 (2007).

79 Snyder, G. J. & Toberer, E. S. Complex Thermoelectric Materials. *Nature Materials* **7**, 105-114, doi:10.1038/nmat2090 (2011).

80 Dirmyer, M. R., Martin, J., Nolas, G. S., Sen, A. & Badding, J. V. Thermal and Electrical Conductivity of Size-Tuned Bismuth Telluride Nanoparticles. *Small* **5**, 933-937, doi:10.1002/smll.200801206 (2009).

81 Jariwala, B., Shah, D. & Ravindra, N. Transport Property Measurements in Doped Bi_2Te_3 Single Crystals Obtained via Zone Melting Method. *Journal of Electronic Materials* **44**, 1509-1516, doi:10.1007/s11664-014-3438-1 (2015).

82 Lee, J.-U. *et al.* Effect of Sn Doping on the Thermoelectric Properties of n-type $Bi_2(Te,Se)_3$ Alloys. *Journal of Electronic Materials* **44**, 1926-1930, doi:10.1007/s11664-014-3598-z (2015).

83 Liu, S. *et al.* Fabrication of Cu-Doped Bi_2Te_3 Nanoplates and Their Thermoelectric Properties. *Journal of Electronic Materials* **46**, 2697-2704, doi:10.1007/s11664-016-4913-7 (2017).

84 Wang, S., Li, H., Lu, R., Zheng, G. & Tang, X. Metal Nanoparticle Decorated n-Type Bi_2Te_3-Based Materials with Enhanced Thermoelectric Performances. *Nanotechnology* **24(285702)**, 1-12, doi:10.1088/0957-4484/24/28/285702 (2013).

85 Han, M. K., Ahn, K., Kim, H., Rhyee, J. S. & Kim, S. J. Formation of Cu Nanoparticles in Layered Bi_2Te_3 and Their Effect on ZT Enhancement. *Journal of Materials Chemistry* **21**, 11365-11370, doi:10.1039/c1jm10163c (2011).

86   Liu, W. S. *et al.* Thermoelectric Property Studies on Cu-Doped n-Type $Cu_xBi_2Te_{2.7}Se_{0.3}$ Nanocomposites. *Advanced Energy Materials* **1**, 577–587, doi:10.1002/aenm.201100149 (2011).

87   Lee, G.-E. *et al.* Preparation and Thermoelectric Properties of Doped Bi_2Te_3-Bi_2Se_3 Solid Solutions.(Report)(Author abstract). *Journal of Electronic Materials* **43**, 1650-1655, doi:10.1007/s11664-013-2822-6 (2014).

88   Yang, J. *et al.* Thermoelectrical Properties of Lutetium-Doped Bi_2Te_3 Bulk Samples Prepared from Flower-Like Nanopowders. *Journal of Alloys and Compounds* **619**, 401-405, doi:10.1016/j.jallcom.2014.09.024 (2015).

89   Hu, L. *et al.* Tuning Multiscale Microstructures to Enhance Thermoelectric Performance of n-Type Bismuth-Telluride-Based Solid Solutions. *Advanced Energy Materials* **5**, 1-13, doi:10.1002/aenm.201500411 (2015).

90   Hu, L., Zhu, T., Liu, X. & Zhao, X. Point Defect Engineering of High-Performance Bismuth-Telluride-Based Thermoelectric Materials. *Advanced Functional Materials* **24**, 5211-5218, doi:10.1002/adfm.201400474 (2014).

91   Zhaojun, X. *et al.* Attaining High Mid-Temperature Performance in $(Bi,Sb)_2Te_3$ Thermoelectric Materials via Synergistic Optimization. *NPG Asia Materials* **8(e302)**, 1-9, doi:10.1038/am.2016.134 (2016).

92   Bludská, J., Jakubec, I., Drašar, Č., Lošťák, P. & Horák, J. Structural Defects in Cu-Doped Bi_2Te_3 Single Crystals. *Philosophical Magazine* **87**, 325-335, doi:10.1080/14786430600990337 (2007).

93   Kavei, G. & Karami, M. A. Formation of Antisite Defects and Bismuth Overstoichiometry in p-Type $Sb_{2-x}Bi_xTe_3$ Thermoelectric Crystals. *Eur. Phys. J. Appl. Phys.* **42**, 67-73 (2008).

94   Zhao, Y., Dyck, J. S., Hernandez, B. M. & Burda, C. Enhancing Thermoelectric Performance of Ternary Nanocrystals through Adjusting Carrier Concentration. *Journal of the American Chemical Society* **132**, 4982–4983, doi:10.1021/ja100020m (2010).

95   May, A. F., Toberer, E. S., Saramat, A. & Snyder, G. J. Characterization and Analysis of Thermoelectric Transport in n-Type $Ba_8Ga_{16-x}Ge_{30+x}$. *Physical Review B - Condensed*

Matter and Materials Physics **80(125205)**, 1-12, doi:10.1103/PhysRevB.80.125205 (2009).

96   Wang, H., Pei, Y. Z., LaLonde, A. D., & Snyder, G. J. *Material Design Considerations Based on Thermoelectric Quality Factor*. Vol. 182 (Springer Berlin Heidelberg, Berlin, Heidelberg, 2013).

97   Ferry, D. K. *Thermoelectric Nanomaterials* (IOP Publishing, 2013).

98   Yu, B. *et al.* Enhancement of Thermoelectric Properties by Modulation-Doping in Silicon Germanium Alloy Nanocomposites. *Nano Letters* **12**, 2077−2082, doi:10.1021/nl3003045 (2012).

99   Zebarjadi, M. *et al.* Power Factor Enhancement by Modulation Doping in Bulk Nanocomposites. *Nano Letters* **11**, 2225–2230, doi:10.1021/nl201206d (2011).

100   Hu, L. P. *et al.* Shifting up the Optimum Figure of Merit of p-Type Bismuth Telluride-Based Thermoelectric Materials for Power Generation by Suppressing Intrinsic Conduction. *NPG Asia Materials* **6(e88)**, 1-8, doi:10.1038/am.2013.86 (2014).

101   Shen, J. J., Hu, L. P., Zhu, T. J. & Zhao, X. B. The Texture Related Anisotropy of Thermoelectric Properties in Bismuth Telluride Based Polycrystalline Alloys. *Applied Physics Letters* **99(124102)**, 1-4, doi:10.1063/1.3643051 (2011).

102   Sun, Z. L., Liufu, S. C., Chen, X. H. & Chen, L. D. Enhanced Thermoelectric Properties of $Bi_{0.5}Sb_{1.5}Te_3$ Films by Chemical Vapor Transport Process. *ACS Appl. Mater. Interfaces* **3**, 1390–1393, doi:10.1021/am200203r (2011).

103   Pei, Y., Lalonde, A. D., Heinz, N. A. & Snyder, G. J. High Thermoelectric Figure of Merit in PbTe Alloys Demonstrated in PbTe-CdTe. *Advanced Energy Materials* **2**, 670-675, doi:10.1002/aenm.201100770 (2012).

104   Pei, Y. Z., Wang, H., Zachary, M. G., Aaron, D. L. & Snyder, G. J. Thermopower Enhancement in $Pb_{1-x}Mn_xTe$ Alloys and Its Effect on Thermoelectric Efficiency. *NPG Asia Materials* **4(e28)**, 1-6, doi:10.1038/am.2012.52 (2012).

105   Tan, G. *et al.* Non-Equilibrium Processing Leads to Record High Thermoelectric Figure of Merit in PbTe-SrTe. *Nature Communications* **7(12167)**, 1-9, doi:10.1038/ncomms12167 (2016).

106   Wang, S. *et al.* High Thermoelectric Performance in Te-Free $(Bi,Sb)_2Se_3$ via Structural Transition Induced Band Convergence and Chemical Bond Softening. *Energy Environ. Sci.* **9**, 3436-3447, doi:10.1039/c6ee02674e (2016).

107   Soni, A. *et al.* Enhanced Thermoelectric Properties of Solution Grown $Bi_2Te_{3-x}Se_x$ Nanoplatelet Composites. *Nano letters* **12**, 1203−1209, doi:10.1021/nl2034859 (2012).

108   Mehdizadeh Dehkordi, A., Zebarjadi, M., He, J. & Tritt, T. M. Thermoelectric Power Factor: Enhancement Mechanisms and Strategies for Higher Performance Thermoelectric Materials. *Materials Science & Engineering R* **97**, 1-22, doi:10.1016/j.mser.2015.08.001 (2015).

109   Fan, S. *et al.* p-Type $Bi_{0.4}Sb_{1.6}Te_3$ Nanocomposites with Enhanced Figure of Merit. *Applied Physics Letters* **96(182104)**, 1-3, doi:10.1063/1.3427427 (2010).

110   *Energy   Filtering   Effect   Model*, <https://www.researchgate.net/figure/263463869_fig7_Figure-5-Schematic-drawing-shows-that-SiC-nanoparticles-in-a-series-of-planes-can-block> (

111   Wang, S. *et al.* On Intensifying Carrier Impurity Scattering to Enhance Thermoelectric Performance in Cr-Doped $Ce_yCo_4Sb_{12}$. *Advanced Functional Materials* **25**, 6660-6670, doi:10.1002/adfm.201502782 (2015).

112   Goldsmid, H. J. Bismuth Telluride and Its Alloys as Materials for Thermoelectric Generation. *Materials* **7**, 2577-2592, doi:10.3390/ma7042577 (2014).

113   Liao, B. L., Maznev, A. A., Nelson, K. A. & Chen, G. Photo-Excited Charge Carriers Suppress Sub-Terahertz Phonon Mode in Silicon at Room Temperature. *Nature Communications* **7(13174)**, 1-7, doi:10.1038/ncomms13174 (2016).

114   Zhu, T. *et al.* The Role of Electron–Phonon Interaction in Heavily Doped Fine-Grained Bulk Silicons as Thermoelectric Materials. *Advanced Electronic Materials* **2(1600171)**, 1-6, doi:10.1002/aelm.201600171 (2016).

115   Duan, B. *et al.* Electronegative Guests in $CoSb_3$. *Energy Environ. Sci.* **9**, 2090-2098, doi:10.1039/c6ee00322b (2016).

116   Shi, X. *et al.* Erratum: Multiple-Filled Skutterudites: High Thermoelectric Figure of Merit through Separately Optimizing Electrical and Thermal Transports. *Journal of the American Chemical Society* **133**, 7837–7846, doi:10.1021/ja111199y (2011).

117   Hao, F. *et al.* High Efficiency Bi$_2$Te$_3$-Based Materials and Devices for Thermoelectric Power Generation between 373 K And 573 K. *Energy Environ. Sci.* **9**, 3120-3127, doi:10.1039/c6ee02017h (2016).

118   Wang, S. *et al.* Enhanced Thermoelectric Properties of Bi$_2$(Te$_{1-x}$Se$_x$)$_3$-Based Compounds As n-Type Legs for Low-Temperature Power Generation. *Journal of Materials Chemistry* **22**, 20943-20951, doi:10.1039/c2jm34608g (2012).

119   Kim, S. I. *et al.* Thermoelectrics. Dense Dislocation Arrays Embedded in Grain Boundaries for High-Performance Bulk Thermoelectrics. *Science* **348**, 109-114, doi:10.1126/science.aaa4166 (2015).

120   Eginligil, M., Zhang, W., Kalitsov, A., Lu, X. & Yang, H. Tunneling Behavior of Bismuth Telluride Nanoplates in Electrical Transport. *Chemical Physics Letters* **546**, 125-128, doi:10.1016/j.cplett.2012.07.068 (2012).

121   Minnich, A. J., Dresselhaus, M. S., Ren, Z. F. & Chen, G. Bulk Nanostructured Thermoelectric Materials: Current Research and Future Prospects. *Energy & Environmental Science* **2**, 466-479, doi:10.1039/b822664b (2009).

122   Yu, F. *et al.* Enhanced Thermoelectric Figure of Merit in Nanocrystalline Bi$_2$Te$_3$ Bulk. *Journal of Applied Physics* **105(094303)**, 1-5, doi:10.1063/1.3120865 (2009).

123   Zheng, Y. *et al.* Mechanically Robust BiSbTe Alloys with Superior Thermoelectric Performance: A Case Study of Stable Hierarchical Nanostructured Thermoelectric Materials. *Adv. Energy Mater.* **5**, 1-11, doi:10.1002/aenm.201401391 (2015).

124   Fu, C. *et al.* Enhancing the Figure of Merit of Heavy-Band Thermoelectric Materials Through Hierarchical Phonon Scattering. *Advanced Science* **3(1600035)**, 1-7 (2016).

125   Xie, W. Unique Nanostructures and Enhanced Thermoelectric Performance of Melt-Spun Bisbte Alloys. *Applied Physics Letters* **94(102111)**, 1-3, doi:10.1063/1.3097026 (2009).

126   Cao, Y. Q., Zhao, X. B., Zhu, T. J., Zhang, X. B. & Tu, J. P. Syntheses and Thermoelectric Properties of Bi$_2$Te$_3$/Sb$_2$Te$_3$ Bulk Nanocomposites with Laminated Nanostructure. *Applied Physics Letters* **92(143106)**, 1-3, doi:10.1063/1.2900960 (2008).

127   Tang, X. *et al.* Preparation and Thermoelectric Transport Properties of High-Performance p-Type Bi_2Te_3 with Layered Nanostructure. *Applied Physics Letters* **90(012102)**, 1-3, doi:10.1063/1.2425007 (2007).

128   Xie, W. *et al.* Identifying the Specific Nanostructures Responsible for the High Thermoelectric Performance of $(Bi,Sb)_2Te_3$ Nanocomposites. *Nano letters* **10**, 3283-3289, doi:10.1021/nl100804a (2010).

129   Zhang, Y., Xu, G., Han, F., Wang, Z. & Ge, C. Preparation and Thermoelectric Properties of Nanoporous Bi_2Te_3-Based Alloys. *Journal of Electronic Materials* **39**, 1741-1745, doi:10.1007/s11664-010-1199-z (2010).

130   Kashiwagi, M. *et al.* Enhanced Figure of Merit of a Porous Thin Film of Bismuth Antimony Telluride. *Applied Physics Letters* **98(023114)**, 1-3, doi:10.1063/1.3543852 (2011).

131   Hamachiyo, T., Ashida, M. & Hasezaki, K. Thermal Conductivity of $Bi_{0.5}Sb_{1.5}Te_3$ Affected by Grain Size and Pores. *Journal of Electronic Materials* **38**, 1048-1051, doi:10.1007/s11664-009-0718-2 (2009).

132   Takashiri, M., Tanaka, S., Hagino, H. & Miyazaki, K. Combined Effect of Nanoscale Grain Size and Porosity on Lattice Thermal Conductivity of Bismuth-Telluride-Based Bulk Alloys. *Journal of Applied Physics* **112(084315)**, 1-8, doi:10.1063/1.4759326 (2012).

Appendices

Appendix A: Synthesis processes used to prepare Bi_2Te_3-based thermoelectric materials

Product	Morphology	Synthetic Method	Precursors	Reaction Atmosphere or Solvent	Growth Temperature (K)	Reference(s)
Bi_2Te_3	Nanorod	Solvothermal	$Bi(NO_3)_3$, K_2TeO_3, $N_2H_4 \cdot H_2O$, $C_2H_8N_2$, $C_{10}H_{16}N_2O_8$	Water	453	36
Bi_2Te_3	Serrate-like nanostructure	Solvothermal	$Bi(NO_3)_3 \cdot 5H_2O$, Na_2TeO_3, ascorbic acid, polyvinyl pyrrolidone, ethylene glycol	Water	473	37
Bi_2Te_3	Nanoplate	Solvothermal	Bi_2O_3, TeO_2, ethylene glycol, polyvinyl pyrrolidone, NaOH	Water	473	38
Bi_2Te_3	Flower-like nanostructure	Solvothermal	$Bi(NO_3)_3 \cdot 5H_2O$, Na_2TeO_3, ethylene glycol, glucose, NaOH, $N_2H_4 \cdot H_2O$	Water	453	42
Sb_2Te_3	Thin film	RF magnetron sputtering	High-purity Sb_2Te_3 alloy	-	Room temperature	44
Bi_2Te_3	Nanocrystalline thin film	RF magnetron sputtering	High-purity Bi_2Te_3	Ar	473	47
Bi_2Te_3	Nanocrystalline thin film	RF magnetron sputtering	Bi(40 at.%)-Te(60 at.%)	Ar	473	48
Sb_2Te_3	Nanocrystalline thin film	RF magnetron sputtering	Sb(40 at.%)-Te(60 at.%)	Ar	473	48
$Bi_{0.5}Sb_{1.5}Te_3$	Thin film	RF magnetron sputtering	High-purity 0.5Bi-1.5Sb-3Te alloy	Ar	Room temperature	49

Bi_2Te_3	Thin film	RF magnetron sputtering	Power mixture of Bi (55 at.%) and Te (45 at.%)	Ar	Room temperature	46
Bi_2Te_3	Nanocrystalline thin film	RF magnetron sputtering	High- purity Bi (30 at.%)-Te (70 at.%) material	Ar	Room temperature	19
Bi_2Te_3	Nanocrystalline thin film	RF magnetron sputtering	High- purity Bi (30 at.%)-Te (70 at.%) material	Ar	Room temperature	50
Sb_2Te_3	Thin film	Thermal evaporation	High-purity Sb_2Te_3 ingot	-	Room temperature to 423 K	51
Bi_2Te_3	Thin film	Thermal evaporation	High-purity Bi_2Te_3 power	-	Room temperature	53
Sb_2Te_3	Thin film	Thermal evaporation	High-purity Sb_2Te_3 power	-	Room temperature	52
$Bi_{0.4}Sb_{1.6}Te_3$	Thin film	Flash evaporation	$Bi_{0.4}Sb_{1.6}Te_3$ power	-	473	54
$Bi_{0.4}Sb_{1.6}Te_3$	Thin film	Flash evaporation	$Bi_{0.4}Sb_{1.6}Te_3$ power	-	473	55
$Bi_{0.4}Sb_{1.6}Te_3$	Thin film	Flash evaporation	$Bi_{0.4}Sb_{1.6}Te_3$ power	-	473	56
$Bi_{2.0}Te_{2.7}Se_{0.3}$	Thin film	Flash evaporation	$Bi_{2.0}Te_{2.7}Se_{0.3}$ power	-	473	56
$Bi_{0.4}Sb_{1.6}Te_3$	Thin film	Flash evaporation	$Bi_{0.4}Sb_{1.6}Te_3$ power	-	473	57
Bi_2Te_3	Thick film	Electrochemical deposition	Bi_2O_3, TeO_2, HNO_3	Water	Room temperature	60
Sb_2Te_3	Thick film	Electrochemical deposition	Sb_2O_3, TeO_2, $C_4H_6O_4 \cdot 5H_2O$, HNO_3	Water	Room temperature	60

Bi_2Te_3	Nanowire	Electrochemical deposition	$Bi(NO_3)_3$, Te, HNO_3, dimethyl sulfoxide	Water	Room temperature	67
$Bi_{0.5}Sb_{1.5}Te_3$	Bulk	Ball milling	Bi, Sb and Te elemental ingots	Ar	Room temperature	32
Bi_2Te_3	Bulk	Ball milling	Bi and Sb elements	N_2	Room temperature	69
$BiSbTe_3$	Bulk	Ball milling	Bi, Sb and Te elemental ingots	N_2	Room temperature	13
$Bi_2Te_{2.7}Se_{0.3}$	Bulk	Ball milling	Bi, Te and Se elemental ingots	-	Room temperature	70
$Bi_2Te_{3-y}Se_y$ (y = 0-0.6)	Bulk	Ball milling	Bi, Te and Se powers	-	Room temperature	33
$Bi_2Te_{3-y}Se_y:I_m$ (y = 0.15-0.6, m=0.0025-0.01)	Bulk	Ball milling	Bi, Te, Se and SbI_3 powers	-	Room temperature	74
$(Bi, Sb)_2Te_3$	Bulk	Ball milling	Bi, Sb and Te elemental ingots	-	Room temperature	73
$(Bi, Sb)_2Te_3$	Nanocrystalline	Ball milling	Crystalline Bi, Sb and Te elemental chunks	Ar	Room temperature	75
$(Bi, Sb)_2Te_3$	Nanocrystalline	Ball milling	Crystalline $(Bi, Sb)_2Te_3$ alloy ingots	Ar	Room temperature	76

Appendix B: Comparison on the synthesis processes of Bi_2Te_3-based thermoelectric materials

Synthetic Method	Advantages	Disadvantages
Solvothermal process	Simple, one-step reaction, cost-efficiency and frequent application in fabricating nanostructures	Difficulties in controlling morphology and purity of nanostructures
Magnetron sputtering	Simple starting materials and cost-efficiency and frequent application in fabricating thin films	Difficulties in controlling stoichiometry
Thermal evaporation	Simple process, time-saving, low fabrication costs and frequent application in preparing thin films	Difficulties in controlling stoichiometry and few previous research work
Flash evaporation	Simple fabrication system and process, low fabrication costs and frequent application in fabricating thin films	Difficulties in obtaining thin films with clean surface
Electrochemical deposition	Simple process, cost-efficiency and applications in manufacturing Bi_2Te_3-based thermoelectric materials with different morphology (such as thick films and nanowires)	Uncertainty of the relationship between atomic composition and applied potentials
Ball milling	Extensive industrial applications, large-quantity manufacture, time-saving and frequent applications in producing bulk and nanostructured materials	Not being able to fabricate films